Journal of Non-Crystalline Solids 355 (2009) 759–775

Contents lists available at ScienceDirect

Journal of Non-Crystalline Solids

journal homepage: www.elsevier.com/locate/jnoncrysol

Review

Rare earth based bulk metallic glasses

Q. Luo, W.H. Wang *

Institute of Physics, Chinese Academy of Sciences, P.O. Box 603, Southern Street 3, No. 8, Zhong Gu, Beijing 100190, PR China

ARTICLE INFO

Article history:
Received 12 August 2008
Received in revised form 11 February 2009
Available online 3 April 2009

PACS:
81.05.Kf
61.43.Dq
75.50.Kj

Keywords:
Amorphous metals
Metallic glasses

ABSTRACT

Recently, the rare earth based bulk metallic glasses (REBMGs) have attracted increasing interest due to their unique properties and potential applications as functional glassy materials. These REBMGs display many fascinating properties such as heavy fermion behavior, thermoplastic properties near room temperature, excellent magnetocaloric effect, hard magnetism, and polyamorphism, all of which are of interest not only for basic research but also for metallurgy and technology. These characteristics and properties are ascribed to the unique electronic, magnetic and atomic structures of the REBMGs. In this review paper, the fabrication, glass-forming ability, polyamorphism, elastic, thermal, and physical properties are summarized and discussed. Owing to the unique electronic structure of rare earth elements, the electric and magnetic properties of the REBMGs are especially addressed. The works have implications for seeking novel metallic glasses with controllable properties and for understanding the nature of glass formation. The development of REBMGs as functional materials might promote and extend the commercial applications of metallic glasses.

1. Introduction

Bulk metallic glasses (BMGs), which open new opportunities for fundamental studies and commercial applications, have attracted world-wide interest. Extensive work has been carried out on the design of new glassy alloys with various unique properties. Many achievements in basic research and applications have been obtained, while many issues remain unresolved. The rare earth (RE) elements have been used as important minor alloying additions and/or main constituent during the development of BMGs [1–5]. In the late 1980s, the Inoue group found exceptional glass-forming ability (GFA) in La–Al–Cu(Ni) alloys [2] and successfully developed fully glassy cylindrical samples with diameters up to 5 mm by Cu mold casting. Later on, bulk glassy Mg–Cu–Y, Mg–Ni–Y and Zr–Al–Ni–Cu alloys were also developed with a low cooling rate of 100 K/s [6,7]. In 1993, the Johnson group developed a $Zr_{41.2}Ti_{13.8}Cu_{12.5}Ni_{10}Be_{22.5}$ alloy (Vit1) with a GFA approaching that of oxide glasses [8]. These works offer a new starting point for BMGs as promising structural and functional materials.

In 1996, rare earth Nd-based bulk metallic glasses (REBMGs) with hard magnetic properties at room temperature (RT) have been developed [9–13]. These hard magnetic properties are ascribed to a unique clustered amorphous structure, while the detailed mechanism is still unclear. In 2003, the Y–Sc–Al–Co REBMGs with diameters up to 25 mm were developed by the Poon group [14] and Pr(Nd)–Al–Ni–Cu REBMGs with diameters of 5 mm were fabricated by our group [15]. With Fe addition, it is found that the Pr-based REBMGs have an inhomogeneous cluster structure (like Nd-based REBMG) exhibiting complex magnetic properties [16]. In 2004, the Ce-based REBMG with ultralow low elastic modulus and glass transition temperature T_g was reported [17,18], and very soon the Ce–Al–Cu (Ni) alloys with diameters up to 12 mm were developed [19,20]. We then systematically investigated the glass formation in the RE-based alloys according to the elastic modulus rule in combination with the classic glass-forming criteria. The work result in the emergence of a series of new Sc-, Gd-, Sm-, Tb-, Dy-, Ho-, Er-, Yb-, Tm- and Lu-based REBMGs with good GFA, high thermal stability and tunable physical and mechanical properties [21–29]. Table 1 lists the properties of RE elements and the typical REBMGs. Later on, extensive work was carried out on the crystallization, glass transition, liquid fragility, GFA, thermal stability, the mechanical and physical properties, elastic properties and their response to temperature, frequency and pressure [30–47].

In this review paper, we systematically summarize the studies on the formation, characteristics, elastic, mechanical and physical properties of these REBMGs. The elastic, electric and magnetic properties of REBMGs are specially addressed because of the unique electronic structure of RE elements. The plentiful phenomena, unique properties and features of these REBMGs is due to the complicated and specific electric and magnetic structure. Through the facility of chemical comparability and property modulation of the base RE elements, we hope to advance our understanding of

* Corresponding author. Fax: +86 10 82640223.
E-mail address: whw@aphy.iphy.ac.cn (W.H. Wang).

0022-3093/$ - see front matter © 2009 Elsevier B.V. All rights reserved.
doi:10.1016/j.jnoncrysol.2009.02.006

Table 1
The Poisson's ratio σ, melting temperature T_m and atomic radius R of rare earth elements, and the typical composition range of REBMG systems [15–29].

Element	σ	R (10^{-10} m)	T_m (K)	Typical REBMGs system
Sc	0.28	1.62	1814	Sc–Al–Co–Y
Y	0.24	1.8	1783	Y–Sc–Al–Co, Y–Al–Co
La	0.28	1.88	1193	La–Al–Ni–Cu, La–Al–Co(Ni)
Ce	0.24	1.83	795	Ce–Al–M(M=Cu, Co, Ni), Ce–Al–Cu–X (X=Co, Nb, B, et al.)
Pr	0.28	1.83	1208	Pr–Fe–Al, Pr–Al–M–N(M, N=Fe, Cu, Ni, Co)
Nd	0.28	1.82	1297	Nd–Al–Fe, Nd–Al–M–N(M, N=Fe, Cu, Ni, Co)
Sm	0.27	1.8	1345	Sm–Al–Co(Ni), Sm–Al–Co–X(X=Y, Nb)
Gd	0.26	1.8	1583	Gd–Al–Co(Fe, Ni), Gd–Al–Ni–Cu (Co), Gd–Y–Al–Co
Tb	0.26	1.78	1629	Tb–Al–Co, Tb–Y–Al–Co
Dy	0.25	1.77	1680	Dy–Al–Co, Dy–Y–Al–Co
Ho	0.23	1.77	1734	Ho–Al–Co, Ho–Y(Zr)–Al–Co
Er	0.24	1.76	1770	Er–Al–Co(Ni), Er–Y–Al–Co(Ni, Fe)
Tm	0.21	1.75	1818	Tm–Al–Co, Tm–Y(Zr)–Al–Co
Yb	0.21	1.93	1092	Yb–Zn–Mg, Yb–Zn–Mg–Cu
Lu	0.26	1.75	1925	Lu–Al–Co, Lu–Y(Zr)–Al–Co

the glassy state, and assist in searching for BMGs and promote their commercial application.

2. The formation of the REBMGs

Table 2 lists the typical compositions of REBMGs studied which were prepared by arc melting and Cu mold cast method. The bulk specimen permits good investigation of various properties, especially the elastic, physical and mechanical properties. The thermal analysis was carried out in a Perkin–Elmer DSC-7 differential scanning calorimeter (DSC) under a purified argon atmosphere. The calorimeter was calibrated for temperature and energy with high purity indium and zinc at the heating rate of 10 K/min. The thermodynamic parameters of glass transition temperature T_g, crystallization temperature T_x, and melting temperature T_m were determined with an accuracy of ±1 K. The isothermal annealing was performed in a furnace under a vacuum of $\sim 1.0 \times 10^{-3}$ Pa at various temperatures. Acoustic velocities were measured in a pulse echo overlap method by a MATEC 6600 model ultrasonic system with a carrying frequency of 10 MHz (error <2%). The measured parameter is the acoustic wave transmitting time in samples, and the measured timing accuracy was 0.5 ns. The density was measured using the Archimedes technique and the accuracy is within 0.5%. The Young's modulus E, shear modulus G, bulk modulus K and Poisson's ratio σ were derived from the density and acoustic velocities. The error was controlled within 3% in the acoustic measurments. The high pressure experiment was performed in a piston-cylinder pressure apparatus. The sample with a bonded transducer was immersed in an electric insulating oil (as the pressure transmitting media, for which hydrostaticity has already been

Table 2
The thermodynamic parameters the critical diameter d_c of typical REBMGs [15–29]. The accuracy of temperature is determined within ±1 K.

Composition	d_c (mm)	T_g (K)	T_x (K)	ΔT_x (K)	T_m (K)	T_l (K)	T_{rg}
$La_{66}Al_{14}Cu_{10}Ni_{10}$	8	404	456	52	656	729	0.554
$Pr_{60}Al_{10}Ni_{10}Cu_{20}$	5	417	469	52	710	725	0.575
$Nd_{60}Cu20Ni_{10}Al_{10}$	5	438	478	40	728	755	0.60
$Ce_{70}Al_{10}Cu_{20}$	2	341	408	67	647	722	0.471
$Ce_{60}Al_{20}Co_{20}$	1	424	468	44	684	798	0.531
$Ce_{68}Al_{10}Cu_{20}Fe_2$	5	352	423	71	646	708	0.497
$Ce_{69.8}Al_{10}Cu_{20}Co_{0.2}$	8	339	414	75	643	721	0.470
$Ce_{69.5}Al_{10}Cu_{20}Co_{0.5}$	10	337	419	82	639	716	0.471
$Ce_{69}Al_{10}Cu_{20}Co_1$	10	340	421	81	634	713	0.477
$Ce_{68}Al_{10}Cu_{20}Co_2$	10	352	419	67	615	716	0.492
$Ce_{65}Al_{10}Cu_{20}Co_5$	8	363	414	51	615	695	0.522
$Ce_{68}Al_{10}Cu_{20}Ni_2$	5	352	421	69	647	710	0.496
$Ce_{70}Al_{10}Cu_{10}Ni_{10}$	3	359	377	18	639	714	0.503
$Ce_{68}Al_{10}Cu_{20}Nb_2$	8	345	421	76	646	721	0.479
$Ce_{70}Al_{10}Cu_{17}Zn_3$	3	341	412	71	634	733	0.465
$Ce_{68}Al_{10}Cu_{20}Si_2$	3	352	413	61	651	721	0.488
$Ce_{68}Al_{10}Cu_{20}C_2$	2	352	406	54	650	723	0.487
$Ce_{68}Al_{10}Cu_{20}B_2$	2	346	393	47	656	731	0.473
$Lu_{45}Y_{10}Al_{25}Co_{20}$	5	698	775	77		1136	0.610
$Er_{36}Al_{24}Co_{20}Y_{20}$	⩾12	661	719	58	1038	1071	0.617
$Tm_{55}Al_{25}Co_{20}$	⩾3	678	733	55	1059	1103	0.6
$Y_{55}Al_{25}Co_{20}$	2	633	694	61	1035	1060	0.597
$La_{55}Al_{25}Co_{20}$	5	477	540	63	712	771	0.619
$Pr_{55}Al_{25}Co_{20}$	5	509	585	76	806	826	0.616
$Nd_{55}Al_{25}Co_{22}$	2	525	593	68	839	859	0.611
$Gd_{55}Al_{25}Co_{20}$	2	585	657	72	949	971	0.602
$Tb_{55}Al_{25}Co_{20}$	3	612	674	62	973	1001	0.611
$Dy_{55}Al_{25}Co_{20}$	3	635	708	73	998	1031	0.616
$Ho_{55}Al_{25}Co_{20}$	3	649	707	58	1035	1055	0.615
$Er_{55}Al_{25}Co_{20}$	⩾5	663	722	59	1056	1079	0.628
$Yb_{62.5}Zn_{15}Mg_{17.5}Cu_5$	4	381	401	20	638		0.575
$Tb_{36}Sm_{20}Al_{24}Co_{20}$	⩾3	582	656	74	932	982	0.593

determined). The measurement was performed in situ for several pressure load–unload cycles to examine the reproducibility and to minimize error. Pressure-induced changes in the sample dimensions were calibrated by using Cook's method. The dynamic mechanical measurement was carried out in a TA DMA2970 thermal mechanical analyzer. The temperature dependence of specific heat, magnetization, isothermal magnetization and the electric resistance were measured in Physical Properties Measurement System (PPMS 6000 of Quantum Design Company).

Due to the unique physical and chemical properties of RE elements, the formation of REBMGs has several features as described as follow:

2.1. Excellent GFA, and large range of T_g, T_x, T_m and tunable properties

In the periodic table, the RE elements possess complicated and specific electric and magnetic structure and form the largest chemically coherent group, which has the facility of chemical and physical comparability as shown in Fig. 1. The versatility and specificity of Sc-, Nd-, Pr-, Gd-, Tb-, Dy-, Er-, Ho-, Tm-, Yb- and Lu-based alloys can be fabricated into fully glassy rods of ~5 mm in diameter indicating the excellent GFA of these RE-based alloys. Critical diameters reaching 30 mm of the full glassy La-based alloys rods, and the Ce-, Y-, Nd-, and Er-based BMGs with thicknesses of several centimeters have also been reported [27,43–47]. Table 2 shows the critical diameters and T_g, T_x, liquidus temperature T_l, supercooled liquid (SL) regions ΔT_x ($=T_x - T_g$) and reduced glass transition temperature T_{rg} ($=T_g/T_l$) of typical REBMGs. For most metallic glasses with excellent GFA, the values of T_{rg} are usually found to be near or larger than 0.6, which is roughly consistent with Turnbull's rule. However, from Table 2 one can see that the classical criteria [4,48–50] do not agree well with the experimental results of the REBMGs. For example, the T_{rg} can be as low as 0.47 for Ce-based REBMGs, which is distinctly smaller than that of all other BMGs with good GFA, and is similar to that of the Al-based (~0.45) and Pd–Si (~0.48) melt-spun glassy ribbons with poor GFA [50,51]. The critical cooling rate (Rc) of $Er_{55}Al_{25}Co_{20}$ is about 40 K/s and less than 250 K/s of $Nd_{55}Al_{25}Co_{20}$, but its ΔT_x (59 K) is smaller than that of Nd–Al–Co (68 K), and the γ ($=T_x/(T_g + T_l)$ = 0.411 [49]) of Er-based REBMG is smaller than that of Gd-based REBMG (γ = 0.422) with poorer GFA [25].

The properties of metallic glasses greatly depend upon the base element, which directly results in various attractive mechanical, chemical, and magnetic properties different from that of Zr-, Cu-, Fe-, Co-, Mg-, and Ca-based BMGs. Likewise, the versatile and well-regulated physical and chemical properties of RE, bring forth peculiar features for REBMGs. A large range of T_g, T_x, T_m and other properties is such an example. The T_g of REBMGs can be as low as near room temperature (RT), and as high as those of Zr-based BMGs. For the listed REBMGs in Table 3, the T_g, T_x, and T_m cover the ranges of ~341–678 K, ~377–760 K, ~615–1130 K, respectively. Importantly, the large ranges of properties can be controlled and are tunable by changing the composition. Previous studies show that the elastic constants have clear relationships with T_g, T_x, and T_l, all of which relate to GFA and the thermal stability of BMGs. On the other hand, the elastic moduli of BMGs depend strongly on their components and can be calculated as a mean value of all elements based on the atomic percents of constituent elements, and thus the elastic properties of BMG can be finely tuned by its constituents [3,5]. These correlations can be applied to control/design properties such as the elastic and mechanical properties of BMGs. Indeed, a series of RE–Al–Co(Ni)–Y(Zr) REBMGs (RE = Gd, Tb, Dy, Ho, Er, Tm, Lu) with better GFA and tunable properties, such as magnetic and mechanical properties, were successfully fabricated in terms of the elastic modulus rule [22–29]. An example is shown in Fig. 2 for the case of $RE_{55}Al_{25}Co_{20}$ series. The REBMGs with a large range and regular property variation are ideal model systems in which to investigate the fundamental issues in glass physics such as GFA, glass transition, thermal stability, crystallization behavior, and the electric and mechanical properties.

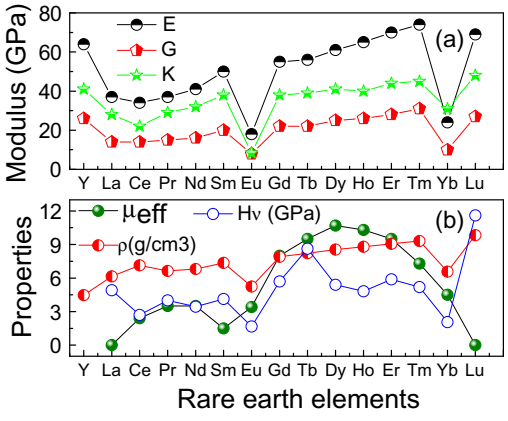

Fig. 1. Typical properties of Young's modulus E, shear modulus G, bulk modulus K, density ρ, Vicker hardness H_v, and effective Bohr magneton moment μ_{eff} for rare earth elements. The solid lines are guides for eyes.

2.2. The GFA and properties of REBMGs are sensitive to minor additions

For REBMGs, their GFA and properties are sensitive to minor element additions. For instance, in Ce-based REBMGs, in addition to their low T_g, their formation is very sensitive to minor addition of Co [19,20]. As shown in Fig. 3(a), dramatic increase of the critical diameter (d_c) from 2 mm to at least 8 mm is observed with 0.2% Co addition (x = 0.2) for $Ce_{70-x}Al_{10}Cu_{20}Co_x$ series. From the inset of Fig. 3(a), one can see that both the ΔT and T_{rg} can not reflect the relative change of GFA. Note that Co has the similar atomic size with Cu, suggesting that the 'confusion principle' and atom size effect alone cannot reflect this subtle influence. A distinct relative 'fragile' to 'strong' transition has be observed by 1% Co micro-alloying in term of the change of $\Delta T_g/T_g$ (a value relates with thermodynamic fragility) and from heat capacity jump near T_g (inset of Fig. 3(b)) [19,52]. This means that the minor addition has obvious impact on the dynamics and stability of the liquid through the microstructural change. The acoustic velocities, Debye temperature and elastic moduli also show abrupt change (relative to the matrix alloy) for the alloy with 0.2% Co addition (Fig. 3). Such large changes of these properties suggest that the alloy falls into a more dense packing structure with significant change of the short-range order due to the minute Co addition. The nuclear magnetic response experiment shows that the symmetry around Al sites is enhanced significantly upon Co addition as reflected by decreasing quadrupole frequency measured by ^{27}Al NMR [53]. The minor addition can stabilize the liquid phase, suppress the crystallization kinetic, and enhance the GFA of REBMGs. Actually, the minor addition has been shown to be a widely used technique to develop novel BMGs with enhanced GFA and properties [3]. However, the underlying mechanism of which is still not fully understood in this field.

2.3. Bulk metallic glasses with multi-bases

The general method to develop BMGs with desired properties is firstly to select proper single base element and match the base element to other glass-forming constituents, and then to improve the GFA though minor addition. For REBMGs there exists a facile

Table 3
The thermodynamic parameters and elastic properties of typical REBMGs with an accuracy of about 3% [15–29].

BMG	T_g (K)	T_x (K)	E (GPa)	G (GPa)	K (GPa)	σ	θ_D (K)
$Ce_{70}Al_{10}Ni_{10}Cu_{10}$	359	377	30.3	11.5	27.0	0.313	144
$(Ce_{20}La_{80})Al_{10}Cu_{20}Co_2$	366	409	30.69	11.33	35.07	0.354	
$(Ce_{50}La_{50})Al_{10}Cu_{20}Co_2$	362	419	31.27	11.60	34.32	0.348	
$Pr_{60}Al_{10}Ni_{10}Cu_{20}$	409	452	37.2	13.6	45.2	0.363	160
$Nd_{60}Fe_{20}Co_{10}Al_{10}$	485	615	54.1	20.7	54.1	0.317	
$Sm_{40}Y_{15}Al_{25}Co_{20}$	590	657	57.1	21.5	54.7	0.326	213
$Gd_{40}Y_{16}Al_{24}Co_{20}$	598	653	62.2	23.5	58.0	0.319	218
$Tb_{36}Y_{20}Al_{24}Co_{20}$	619	686	63.6	24.0	60.5	0.325	222
$Dy_{46}Y_{10}Al_{24}Co_{20}Fe_2$	627	682	64.2	24.4	58.5	0.317	214
$Ho_{39}Al_{25}Co_{20}Y_{16}$	649	706	69.1	26.2	63.6	0.319	
$Er_{50}Y_6Al_{24}Co_{20}$	651	702	71.0	27.0	65.1	0.318	218
$Sc_{36}Y_{20}Al_{24}Co_{20}$	662	760	85.2	32.3	77.5	0.317	337
$Tm_{39}Y_{16}Al_{25}Co_{20}$	664	735	77.5	29.7	66.1	0.304	238
$Tm_{45}Y_{10}Al_{25}Co_{20}$	672	734	71.5	27.3	62.3	0.309	223
$Tb_{36}Ho_{20}Al_{24}Co_{20}$	617	672	62.7	23.8	57.2	0.317	
$Tb_{36}Er_{20}Al_{24}Co_{20}$	622	677	64.5	24.3	61.7	0.326	
$Yb_{62.5}Zn_{15}Mg_{17.5}Cu_5$	381	401	26.5	10.4	19.8	0.276	132
$Lu_{45}Y_{10}Al_{25}Co_{20}$	698	775	79.1	31.1	70.2	0.309	231

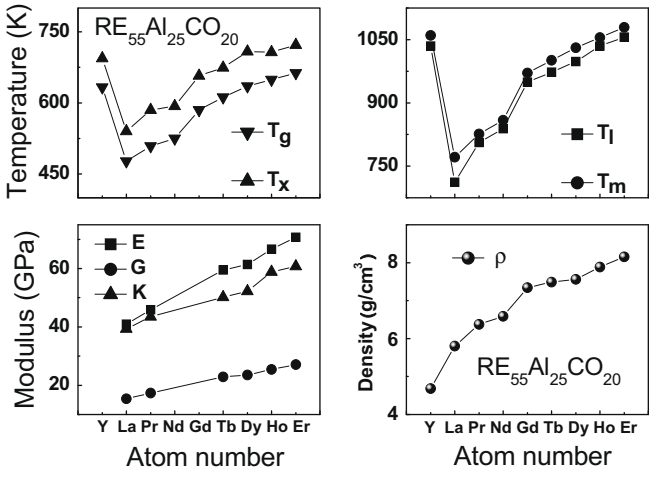

Fig. 2. The dependences of T_g, T_x, T_m, T_l and elastic constants upon the atomic number of RE for the as-cast $RE_{55}Al_{25}Co_{20}$ REBMGs. The solid lines are guides to eyes.

multi-bases formation strategy of fabrication of alloys with controlled properties. It is found that the REBMGs usually can based on two or more RE elements owing to the physical coherency and comparability of RE elements, and the ratio of the REs can be arbitrarily changed over a large composition range (in this sense we call them multi-bases), which is not ordinary for transitional elements families such as Zr-, Fe-, Co-, Ni- and Cu-based BMGs. For example, the misch metal (including La, Ce, Pr, Nd, etc.) based BMGs with modulated thermoplastic and mechanical properties can be readily formed. And it is found out that the GFA, fragility, elastic and electric properties of LaCe-based BMGs could be modulated by gradually changing the ratio of two bases of La and Ce in a range of 0–1 [35,44]. The heavy fermion behavior and magnetocaloric effect of REBMGs can also be readily tuned or even enhanced by binary RE bases formation [46,47]. In particular, the availability of REBMGs with well-regulated mechanical and physical properties, via multi-bases formation strategy, can assist in the investigation of the some correlations among the properties and elastic constants, and permit a better understanding of the electric and magnetic properties. Besides, the tunable and improved thermoplastic properties, hard magnetic properties and magnetocaloric effect of REBMGs could extend the applications of metallic glasses as functional materials.

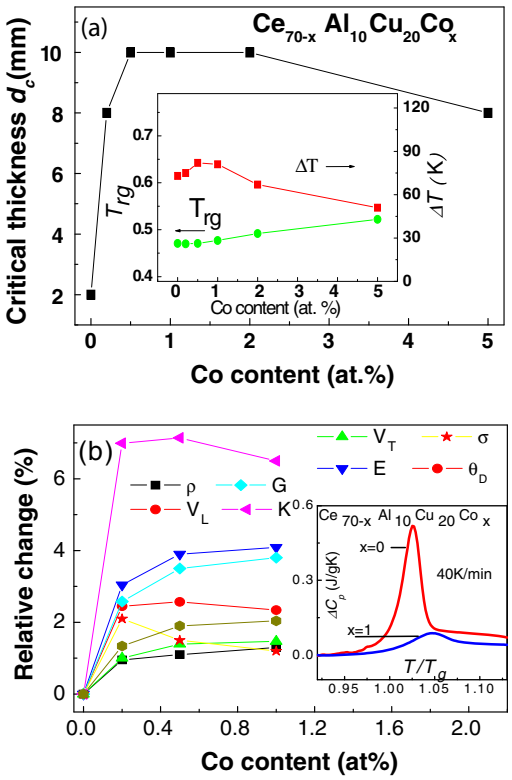

Fig. 3. (a) The relation between the critical diameter (d_c) and Co content. The inset shows the changes of T_{rg} and ΔT. The solid lines are guides for eyes. (b) Relative changes of the density, elastic moduli and Debye temperature for the Co microalloyed REBMGs with respect to the matrix REBMG. The inset is the DSC traces near glass transition temperature for $Ce_{70}Al_{10}Cu_{20}$ and $Ce_{69}Al_{10}Cu_{20}Co_1$ [19].

3. Unique properties and features of REBMGs

The specificity and versatility of RE-based alloys have given them a high level of technological, environmental, and economic importance. For example, samarium–cobalt and iron–neodymium–boron alloys are known for their excellent stability of magnets with high remanence and coercive field strengths. These magnets form an integral part of hard disk drives, electric motors, and compact headphones. The RE–TM (TM is transitional metal) amorphous films are known for their magnetic recording and

memory applications. As the newcomers, the REBMGs have already displayed many unique and attracting properties and features, which are of fundamental interest and promising for engineering and/or functional applications.

3.1. Polymerlike thermoplastic behavior of Ce(La)-based REBMGs

Fig. 4(a) shows the DSC traces of $Ce_{70}Al_{10}Cu_{20}$ and $Ce_{68}Al_{10}Cu_{20}Nb_2$ REBMGs. The T_g of $Ce_{70}Al_{10}Cu_{20}$ is determined to be 68 K, which is lower than the boiling point of water and much lower that of many other BMGs (Fig. 4(b)). Note that the T_g of the two alloys is close to that of some amorphous polymers, such as nylon (~316 K), and even lower than that of polyvinylchloride (348–423 K) [17–20]. And the stability of Ce-based REBMGs both in the supercooled liquid and the glass states has been proved by DSC and aging experiments. The large values of ΔT_x ($\Delta T_x = 80$ K for $Ce_{68}Al_{10}Cu_{20}Nb_2$) and γ of these alloys are obtained indicating the good stability of supercooled liquid and good GFA of these alloys. For $Ce_{70}Al_{10}Cu_{20}$, it is found that the time before crystallization is about 9 h at 358 K in the deep supercooled liquid state, and the predicted lifetime at 293 K with Arrhenius extrapolation is about 200 years [17–20]. The metallic glasses with low T_g normally are quite unstable [1]. Because of the very low T_g of the Ce-based REBMGs, its aging behavior is of concern. As shown in Fig. 5, the fully glass state of Ce-based REBMG is retained even after 147 h annealing at 333 K (10 K below T_g) [54]. The increasing overshot in Fig. 5 indicates a progressive evolution to a denser and lower energy metastable state accompanied by the annihilation of excess free volume with increasing annealing time. Whereas, only minute changes of density, acoustic and elastic properties during the prolonged annealing were observed [54], which indicates that the long time aging only leads to local structure relaxation, and does not induce negative influence on the thermoplastic and mechanical properties of these REBMG, which is important for guaranteeing the applications.

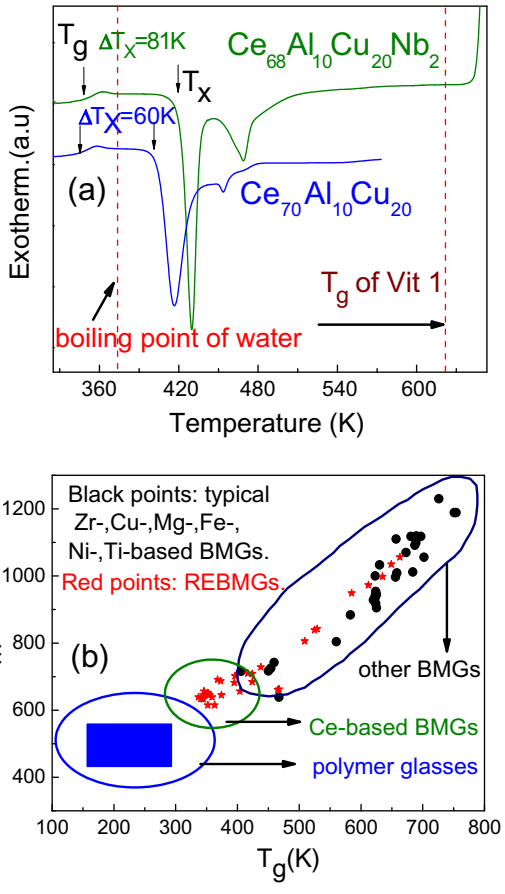

Fig. 4. (a) DSC traces at a heating rate of 10 K min^{-1} for $Ce_{70}Al_{10}Cu_{20}$ and $Ce_{68}Al_{10}Cu_{20}Nb_2$ glasses showing the low T_g (341 K). (b) Relation between T_g and T_m for Ce-based metallic plastic, other BMGs and polymer glasses.

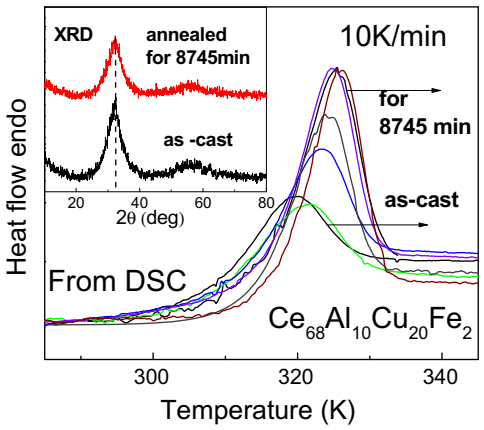

Fig. 5. Enthalpy recovery change of the REBMG as function of annealing time measured by DSC for $Ce_{68}Al_{10}Cu_{20}Fe_2$.The inset shows XRD patterns of the as-quenched and annealed (at 333 K for 8745 min) states [54].

The most attractive feature of Ce-based REBMGs is the temperature-driven transition from metallic-like to plastic-like behavior. At RT, even so close to T_g in the glass state, the alloys is strong and brittle, showing 1.5% elastic strain followed by catastrophic failure in compression. However, on raising the temperature to only near the boiling point of water (Fig. 6), the alloys become soft and can be repeatedly compressed, stretched, bent, and formed into complicated shapes. This thermoplastic processing, shaping and forming at such a low temperatures near 373 K are unusual for conventional metallic materials. Compared with the thermoplastic behavior in supercooled liquid states of other BMGs with high T_g, the Ce-based REBMGs possess remarkable energy saving advantages in production. Significantly, for the amorphous metallic plastics, due to the lack of crystallinity and solidification shrinkage, they can replicate very fine microstructures even in the nanometer scale. This is of great importance for microelectro-mechanical systems and other areas where high precision parts are needed. As shown in Fig. 7, the precise patterns demonstrate that the REBMGs can be used as potential materials for micro- and nano-manufacturing.

Compared with most of polymers, the advantage of the metallic plastic is that when it is returned to room temperature after thermoplastic treatment it resumes typical metallic alloy behavior such as high strength and good electric conductivity. As an example for $Ce_{68}Al_{10}Cu_{20}Nb_2$, the density (6.738 Mgm^{-3}), elastic modulus, Vickers hardness ~1.50 GPa, fracture toughness ~10.0 $MPam^{1/2}$, Poisson's ratio ~0.32, and tensile strength ~490 MPa all are much higher than those of typical polymers [17,18]. And the electrical resistivity of this REBMG is ~119 μΩ cm indicating its metallic conductivity, in contrast to the insulating properties of typical polymers. Although cerium metal oxidizes readily even at RT, the new Ce–Al–Cu–(Nb) REBMGs maintain a good surface finish, thus appearing to be oxidation and corrosion resistance, which are favored for applications such as micro-machines in nanoimprint lithography. Note that the anti-oxidation ability degrades in the supercooled liquid compared with the glassy state of the Ce-based alloys, thus new Ce-based REBMGs with higher anti-oxidation ability and other families of BMGs with similar advantageous thermoplastic properties are desired.

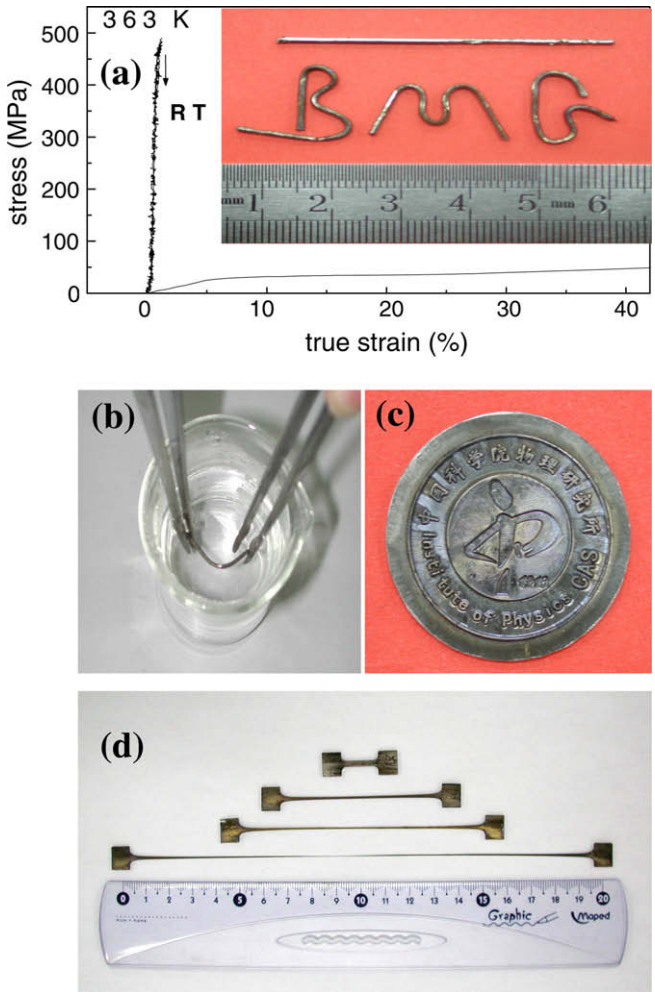

Fig. 6. (a) True stress–true strain curve of a 2 mm-diameter $Ce_{70}Al_{10}Cu_{20}$ glassy rod tested under a compression at RT and at 363 K (90 °C). The inset shows the glassy rods formed into letters by simple manipulation in near-boiling water as shown in (b). (c) Articles for the badge of the Institute of Physics of Chinese Academy of Sciences held in near-boiling water, demonstrating excellent imprintability and viscous deformability. (d) The starting and elongated samples of $Ce_{69}Al_{10}Cu_{20}Co_1$ metallic plastic [45].

The thermoplasticity results from the glassy structure with low T_g, which is well correlated to the excellent GFA and its low moduli of the BMG as seen in Fig. 8, which shows the relation between K and E for Ce-based REBMGs, other BMGs, oxide glasses and conventional crystalline alloys. The metallic conductivity arises from the metallic bonding nature. The good mechanical performance compared with typical polymers can be attributed to the metallic amorphous structure. Additionally their high thermal stability with a large supercooled liquid region provides practical time and temperature scales for heat treatment and thermoplastic processing. By using the elastic modulus rule for smart selection of components with suitable elastic moduli, new polymer-like BMGs (La-, CeLa-, Yb-, Au-, Ca-based alloys) with excellent thermoplastic properties for promising applications as high-performance micro-structures and micro-machines have also been developed [29].

3.2. Hard magnetic properties of Nd(Pr)-based REBMGs

So far, the hard magnetic property has been found to exist only in the Fe-rich Nd (Pr) based alloys, and the Fe-free Nd-based BMGs such as Nd–Al–Co and Nd–Al–Ni–Cu systems show paramagnetic properties at RT [10–12,40]. Furthermore, the coercivity of the ferromagnetic alloys depends strongly on the cooling rate or production methods, indicating the subtle relationship between the structural and magnetic characters. It has been reported that the coercivity of as-cast bulk $Nd_{60}Fe_{30}Al_{10}$ alloy is about 277 kA/m at RT, whereas the same melt-spun ribbons exhibit softer magnetic behavior with H_c of only several kA/m [55]. The hard magnetism doesn't change significantly with annealing around T_g but usually disappear when the samples are completely crystallized [9,13]. Although it is generally accepted that the large coercivity is attributed to a variety of different metastable phases (or clusters) and microstructure, the interplay between the local structures and magnetism remains controversial [9–13,55–60].

Nano scale clusters consisting of Nd and/or transitional metals are generally observed by high resolution transmission electron microscopy, Mössbauer spectra measurements, magnetic and resistance measurements, and isothermal calorimetry investigation, etc., in Nd- and Pr-based glasses [9–13,55–65]. Schneider et al. attributed the intrinsic composite structure to a phase separation process taking place in the melt or the supercooled liquid state [55–57]. Sun et al. shown the existence of two amorphous magnetic phases in melt-spun $Nd_{60-x}Y_xFe_{30}Al_{10}$ ($x = 0, 10, 30$) ribbons [66,67]. McCallum, et al. observed antiferromagnetic motes coupled with the ferromagnetic matrix in amorphous Nd-based alloys [68]. Experimentally, the microstructure of Nd–Fe based glasses is sensitive to the preparation condition, which usually leads to different micro-structures observed in the same composition by different authors. Based on the cluster model of Nd–Fe magnetic system, Inoue et al. interpreted the hard magnetic behavior of these alloys as the magnetic exchange coupling interaction among the magnetic clusters with large random anisotropy [9–12]. The large random magnetic anisotropy (RMA) constrains the vector of magnetic moment in the orientation of local anisotropy. Hard magnetic properties can be expected through exchange coupling among clusters and when the cluster size matches the single domain size. The presence of the exchange coupling interaction between short-scale ordered magnetic atomic clusters is confirmed by the magnetic-force images in $Nd_{60}Al_{10}Fe_{20}Co_{10}$ BMG [13]. Besides the paramagnetic phases, the grains boundaries, surfaces and magnetic inhomogeneities can play an important role as pinning sites of domain walls. The strong domain wall pinning mechanism (the pinning criterion is satisfied when: $a \gg \delta^2$, where a is the lateral area of a single pin and δ is the wall width [65]) has been proved in these Nd-based alloys from the temperature dependence of coercivity [55–60,69]. This is because that the condition of large impediments and narrow domain walls (small δ) are easily favored by the inhomogeneous structure and the large RMA in the Nd-based alloys.

Therefore, there are competing mechanisms dominating the coercivity of Nd-based glasses. Generally the exchange coupling interactions of the magnetic clusters with RMA determine the coercivity in the high temperature region. With decreasing temperature the coercivity increases indicating that the thermal activated pinning mechanisms are gradually dominating the enhancement of the coercivity, until the pinning clusters become magnetic ordered. Since the exchange coupling, large magnetic anisotropy and the pinning mechanism are sensitive to the morphology and composition of various clusters, it is reasonable that the magnetic properties of these alloys are strongly dependent on the cooling rate. For bulk sample fabricated with lower cooling rates than ribbons, the atoms have more time to rearrange and diffuse for a lower energetic configuration, and thus a variety of atomic clusters with a certain degree of short-range or medium-range order may be formed. As the number and size of clusters increase, the exchange couplings are strengthened, and pinning centers become more facile.

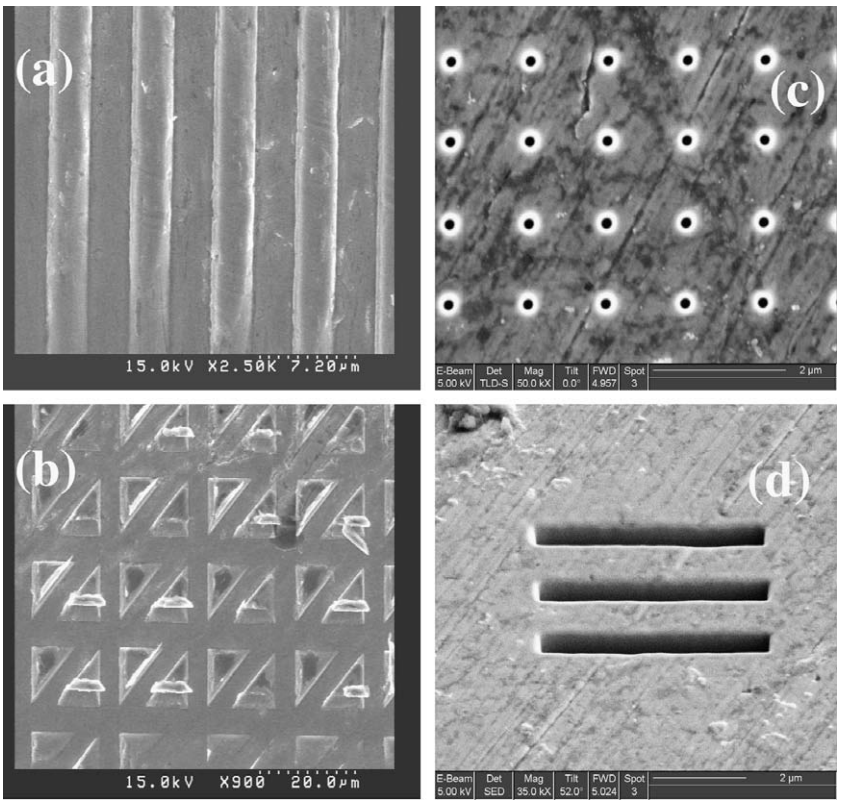

Fig. 7. SEM pictures of the rectangular strip (a) and triangular (b) patterns by microforming on the surface of $Ce_{68}Al_{10}Cu_{20}Co_2$ using silicon die, and SEM pictures of the 4 × 5 array (c) and the groove (d) fabricated on the surface of the metallic plastic sample using the FIB etching technology [20].

3.3. Magnetocaloric effect in REBMGs

Recently there is increasing interest in glassy materials for application as magnetic refrigerants [46,47,70–78,80–84,79,85]. Promising REBMG candidates for this application have recently been confirmed by our investigations [46,47,74]. Typical temperature dependence of magnetization for $Gd_{51}Al_{24}Co_{20}Zr_4Nb_1$ and $Gd_{55}Ni_{25}Al_{20}$ under a magnetic field of 200 Oe is shown in Fig. 9(a). For both alloys, the magnetization varies sharply at the ordering temperature suggesting a homogeneous structure. Fig. 10 shows the magnetic entropy change, $-\Delta S_m$, of typical Gd-based REBMGs. For all the samples, the position of the maximum of $-\Delta S_m$ is located in the vicinity of the transition temperature, and the peak values of $-\Delta S_m$ are 9.40 J kg^{-1} K^{-1} at 93 K, and 9.23 J kg^{-1} K^{-1} at 92.5 K for $Gd_{53}Al_{24}Co_{20}Zr_3$ and $Gd_{51}Al_{24}Co_{20}Zr_4Nb_1$, respectively. In addition to the small magnetic hysteresis over the temperature range investigated, it is worth noting that the large value of $-\Delta S_m$ covers a much broader temperature range compared with most crystalline materials [46,47]. This directly results in an increased refrigerant capacity (RC) of 590 and 651 Jkg^{-1} for $Gd_{53}Al_{24}Co_{20}Zr_3$ and $Gd_{51}Al_{24}Co_{20}Zr_4Nb_1$, respectively, which are much larger than those of $Gd_5Si_2Ge_2$ (305 Jkg^{-1}) and $Gd_5Si_2Ge_{1.9}Fe_{0.1}$ (360 Jkg^{-1}). The RC can be calculated by different methods [46,73,86]. In this paper RC is determined by numerically integrating the area under the ΔS_m–T curve, using the temperatures at half-maximum of the peak as the integration limits. The better RC favored by practical usage in Ericsson-cycle, associates with the large magnetic moment of the alloys and their amorphous structure which extends the large MCE to a wider temperature range.

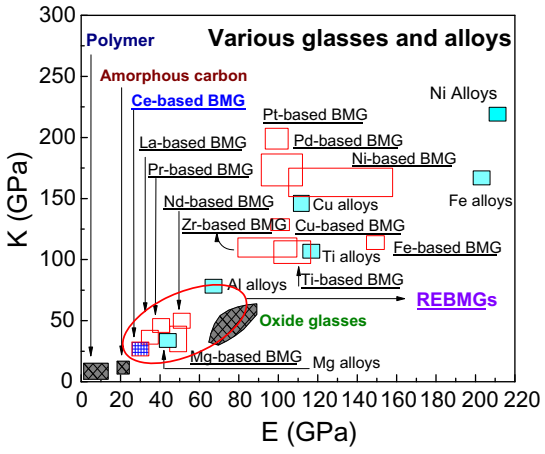

Fig. 8. The relation between K and E for Ce-based REBMGs and others, oxide glasses and conventional crystalline alloys.

Unlike the Gd-based REBMGs, the Ho-, Dy-, Tb- and Er-based REBMGs possess moderate or strong RMA resulting in the lack of long range ferromagnetic order (Fig. 9(b)). Because of the RMA, at low temperature all the Ho-, Dy-, Tb-, Er- based REBMGs show spin-glass-like behavior with obvious hysteresis, indicating that these alloys are magnetically harder than that of Gd-based REBMGs. However, near and above T_f (spin freezing temperature), no magnetic hystersis is observed in the paramagnetic (superparamagnetic) region [54]. Furthermore, it is found that the maximums of $-\Delta S_m$ for Dy-, Ho- and Er-based REBMGs (Fig. 11) are comparable with, or even larger than, those of intermetallic alloys such as $DyAl_2$, $DyNi_2$, $Dy_{1-x}Er_xAl_2$ and $Tb_xY_{1-x}Al_2$ [87,88]. The MCE properties of REBMGs and other materials are presented in Table 4 for comparison. In a word, the REBMGs prossess a tailorable ordering temperature, higher electrical resistivity and thus smaller eddy

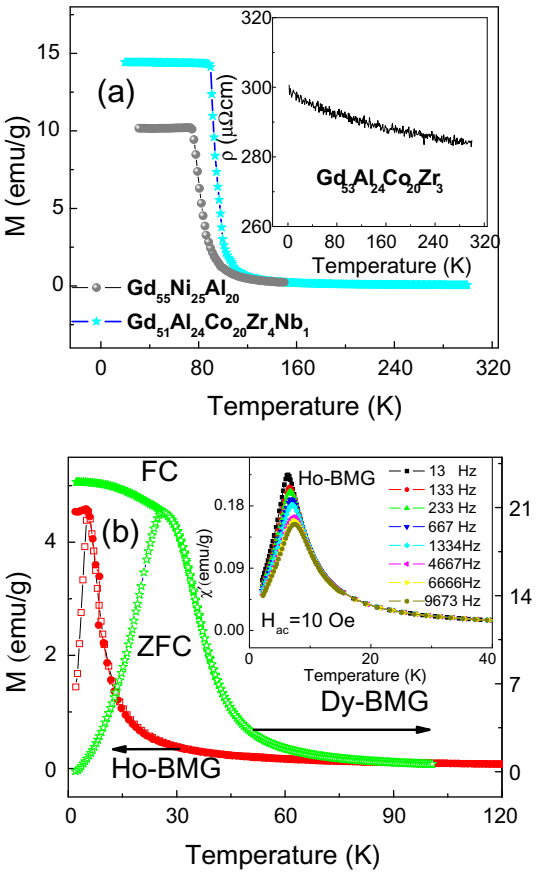

Fig. 9. (a) Temperature dependence of the magnetization curves under 200 Oe for $Gd_{51}Al_{24}Co_{20}Zr_4Nb_1$ and $Gd_{55}Ni_{25}Al_{20}$. The inset shows the electric resistivity of $Gd_{53}Al_{24}Co_{20}Zr_3$. (b) Temperature dependence of ZFC (open plots) and FC (filled plots) magnetization under 500 Oe for $Dy_{50}Gd_7Al_{23}Co_{20}$ and 200 Oe for $Ho_{30}Y_{26}Al_{24}Co_{20}$. The inset shows the ac susceptibility of $Ho_{30}Y_{26}Al_{24}Co_{20}$.

current heating, and high corrosion resistance. Compared with the glass ribbons, these bulk specimens particularly possess low fabrication cost, outstanding mechanical properties and a large supercooled liquid region convenient for heat treatment.

The MCE of crystalline materials are strongly dependent on the structure [70]. For BMGs, the structure can be modulated by controlling the aging and crystallization progress. We find that aging

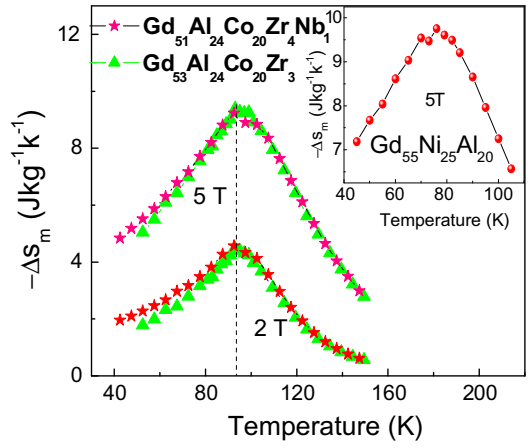

Fig. 10. Magnetic entropy changes for the as-cast $Gd_{51}Al_{24}Co_{20}Zr_4Nb_1$ and $Gd_{53}Al_{24}Co_{20}Zr_3$. The inset shows that of Gd_{55} $Ni_{25}Al_{20}$ under a filed change of 5 T. The solid lines are guides for eyes.

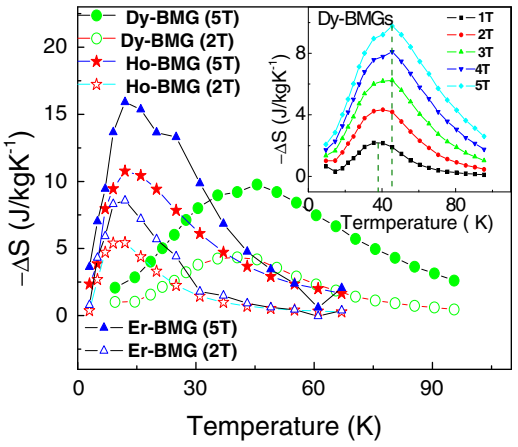

Fig. 11. Magnetic entropy changes for the as-cast $Ho_{30}Y_{26}Al_{24}Co_{20}$, $Dy_{50}Gd_7Al_{23}Co_{20}$ and $Er_{50}Al_{24}Co_{20}Y_6$. The inset shows the magnetic entropy changes under different of fields for $Dy_{50}Gd_7Al_{23}Co_{20}$. The solid lines are guides for eyes.

and crystallization have obvious impacts on MCE of REBMGs indicating its sensitivity to microstructure. The aging sample was annealed at 573 K (T_g = 598 K) for 30 h, the full crystallized sample was annealed at 923 K for 5 h and the two partially crystallized samples were annealed at 613 K for 1 h and 703 K for 1 h. XRD patterns indicated that the aging sample was still amorphous, the full crystallized sample was composed of multi-crystalline phases and the samples annealed in supercooled liquid region contained slightly crystallized phases embedded in amorphous matrix. In contrast to the sharp transition near T_c of the as-cast sample, the magnetic transition is smeared out obviously for all the treated samples as shown in Fig. 12(a). From Fig. 12(b) after long time aging below T_g, the $-\Delta S_m$ reduces and the cusp also moves to lower temperature. The reduction is associated with the atom and stress relaxation to a more stable state companied with atoms rearrangement and increasing of the size of nano-scale clusters. Similarly the crystallization, partially or fully, always results in a remarkable reduction of $-\Delta S_m$. Nevertheless, the reduced values are still much larger than those of the Fe (Co)-based glass ribbons [77,78,80]. Interestingly, it is found that partially devitrification of the BMGs with nanocrystalline grains embedded in amorphous matrix results in an almost constant (table-like, see Fig. 12(b)) and relatively high magnetic entropy change over a large temperature range. This is favored by practical application in Ericsson-cycle, in which ideal magnetic refrigerants having a constant $-\Delta S_m$ through the thermodynamical cycle range are needed. Usually, multilayered structure materials are designed to meet this requirement [89–91], where ferromagnetic materials with varying Curie temperature are layered or sintered. Compared with the method of using layered or sintered composites, the crystallization method owns its biggest advantage of convenience and makes the construction of active magnetic regenerator much simpler. To further tune MCE, the effect of alloying is investigated for Gd-based REBMGs. Fig. 13(a) shows the magnetic entropy change of these alloys from which it can be seen that the alloying effects of Ce, Er and Cr can only tune the position of the peak of $-\Delta S_m$ without changing the peak value and the RC of the alloy. The slightly reduction of the peak value of $-\Delta S_m$ for B additional alloy are due to few crystalline phase in the amorphous matrix, similar to the partially crystallization effect. Our study shows that alloying does not bring negative impact on the MCE, however it can act as a useful tool to tune the working temperature. A comparison of magnetic entropy change among REBMGs and other materials are shown in Fig. 13(b).

Table 4
Magnetic entropy changes and related parameters for various materials. The *a*, *c* and *a* + *c* stand for the amorphous, crystalline and crystalline phases embedded in the amorphous matrix, respectively. The RC values are calculated by the same method.

Material	Structure	Applied field (T)	Peak of ΔS_m (J kg^{-1} K^{-1})	Transition temperature (K)	Refrigerant capacity (Jkg^{-1})	Reference
$Gd_{53}Al_{24}Co_{20}Zr_3$	*a*	5	9.4	93	590	[46]
$Gd_{55}Ni_{25}Al_{20}$	*a*	5	9.76	79	–	[74]
$Gd_{33}Er_{22}Al_{25}Co_{20}$	*a*	5	9.47	52	574	[46]
$Gd_{51}Al_{24}Co_{20}Nb_1Cr_4$	*a*	5	9.48	100	611	[74]
$Gd_{51}Al_{24}Co_{20}Nb_1B_4$	*a* + *c*	5	7.98	74–90	504	[74]
$Gd_{48}Al_{25}Co_{20}Zr_3Er_4$	*a*	5	9.41	84	647	[74]
$Gd_{51}Al_{24}Co_{20}Zr_4Nb_1$	*a*	5	9.23	91	651	[74]
$Gd_{51}Al_{24}Co_{20}Ce_5$	*a*	5	8.85	81	679	[74]
$Gd_{30}Al_{25}Co_{20}$ $Y_{20}Zr_5$	*a*	5	7.64	37	413	[74]
$Ho_{30}Y_{26}Al_{24}Co_{20}$	*a*	5	10.76	5.5	241	[47]
$Dy_{50}Gd_7Al_{23}Co_{20}$	*a*	5	9.77	26	290	[47]
$Er_{50}Al_{24}Co_{20}Y_6$	*a*	5	15.91	8	423	[47]
$(Er_{0.7}Ho_{0.2}Dy_{0.1})_{55}Ni_{25}Al_{20}$	*a*	5	14.02	3	277	[74]
$Tb_{36}Y_{20}Al_{24}Co_{20}$	*a* + *c*	5	5.60	30	–	[74]
$Gd_{60}Co_{26}Al_{14}$	*a*	5	10.1	79	557	[83]
$Gd_{36}Er_{20}Al_{24}Co_{20}$	*a*	5	13.86	–	474	[74]
$Gd_{36}Y_{20}Al_{24}Co_{20}$			7.76	–	459	[74]
Gd	*c*	5	9.8	293	–	[70]
$Gd_5Si_2Ge_2$	*c*	5	18.6	276	306	[73]
$Gd_5Si_2Ge_{1.9}Fe_{0.1}$	*c*	5	7	276	360	[73]
$La_{0.8}Ca_{0.2}MnO_3$	*c*	1.5	5.5	230	66	[71]
$Ni_2Mn_{0.75}Cu_{0.25}$ Ga	*c*	5	65	308	72	[72]
$MnFeP_{0.45}As_{0.55}$	*c*	5	18.3	306	390	[72]
$Fe_{70}B_5C_5Si_3Al_5Ga_2P_{10}$	*a*	1.5	1.65	~588	74	[80]
$Fe_{60}Cr_{14}Cu_1Nb_3Si_{13}B_9$	*a*	3	0.9	226	38	[77]

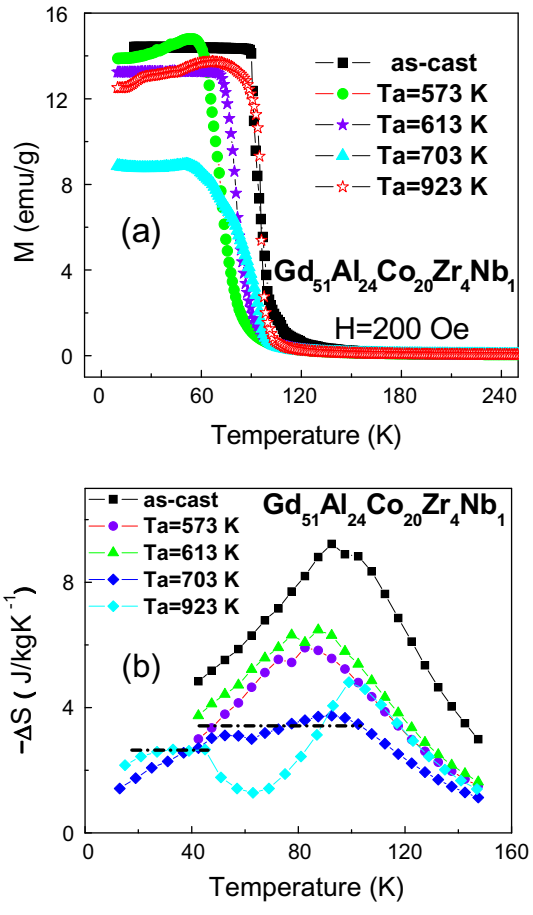

Fig. 12. (a) Temperature dependence of the magnetization curves under 200 Oe for the as-cast and the annealed samples of $Gd_{51}Al_{24}Co_{20}Zr_4Nb_1$. (b) Magnetic entropy changes under a field change of 5 T. The dashed straight lines are guides for eyes.

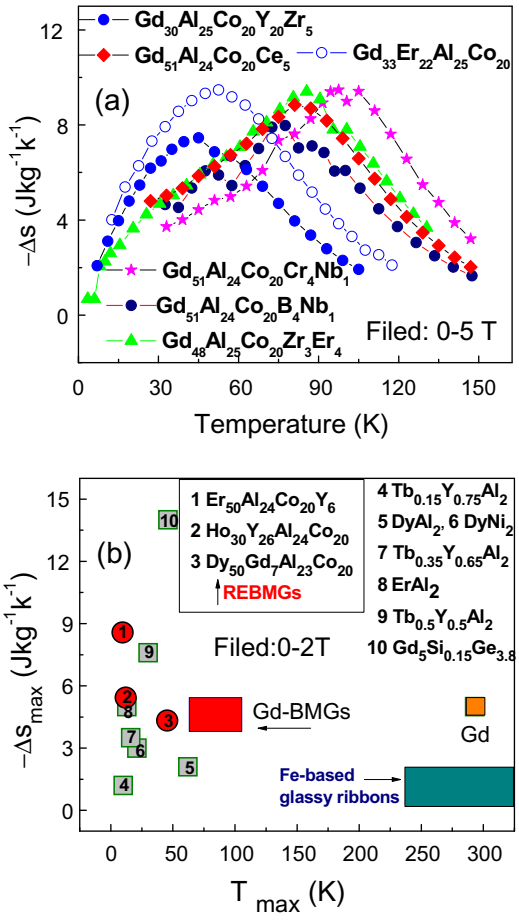

Fig. 13. (a) Magnetic entropy changes for six alloying Gd-based REBMGs under filed change of 5 T. (b) Maximal entropy change of various materials at a field change of 2 T.

The REBMGs exhibit large MCE over a relatively wider temperature range compared with many crystalline materials. Generally, $RE_xR_yAl_aT_zM_{100-a-x-y-z}$ series (RE is the heavy rare earth element, R is Y, Zr or another rare earth element, T is Co or Ni, M is any minor addition element) with controllable transition temperature in a large range and excellent MCE can be fabricated, and the REBMGs can also be mixed/layered to get nearly constant $-\Delta S_m$ over a broad temperature range. The working temperature range could be extended to RT with the development of more REBMGs. The devitrification of BMGs is a promising route to prepare nanocrystalline materials with improved properties. Compared with the multilayered structure, the glassy alloys and corresponding crystallized composites have the merits of low cost and much facility in manufacture without the problem of solid-state reactions between constituent materials which is usually encountered in multilayered materials.

3.4. Elastic properties of REBMGs and the polyamorphism

The elastic properties provide critical information about the bonding characteristics and microstructure of BMGs [92–104]. It has been found that the elastic modulus of a BMG is related to the weighted average of elastic constants for its constituents [105–109]. Furthermore, some established correlations between elastic moduli and various properties such as glass transition, crystallization, GFA, mechanical properties, and even the liquid fragility have been found [105–117,52,118–121]. It has been reported that the fracture tensile strength and compressive yield strengths show a clear linear relationship with E and G, respectively [109–111]. The correlation of Vicker's hardness H_v and E for $RE_{55}Al_{25}Co_{20}$ REBMGs as an example is shown in the inset of Fig. 14(b). Fig. 14 also shows the relationship between $T_g(T_x)$ and elastic modulus for more than 20 REBMGs. This linear response indicates that the thermal stability of REBMGs, the nature of the glass transition and the crystallization characteristics are related to elastic modulus of the materials [105,111–114]. Interestingly, an apparent correlation between θ_D and T_g is reported [115–117], indicating that the glass transition of the BMG-forming alloys even has the softening characteristic of melting [115–117]. Such a rough correlation for REBMGs is shown in Fig. 15. The empirical criteria for evaluating the GFA, such as T_{rg}, and ΔT_x are usually based on these characteristic temperatures (T_g, T_x, T_l and T_m), all of which are related to elastic moduli. This implies that elastic constants can be used to monitor and control the GFA and properties in BMGs. This has indeed been observed and applied to the design of new BMGs in our group and some others. At present, a comprehensive understanding of the above correlations is far from complete, and remains a topic of intense for research.

Temperature and pressure dependences of acoustic and elastic behaviors are of significance for the general understanding of the microstructure and vibration features of BMGs [122–125]. For typical La-, Mg-, Cu-, Zr-based BMGs in Fig. 16, it has been found that both the longitudinal acoustic velocity, V_L, and transverse acoustic velocity, V_T, increase roughly linearly with decreasing T. However, the behavior of Ce-based REBMGs shows remarkably obvious softening of V_L with decreasing temperature (the inset of Fig. 16(a)), which suggests possible amorphous to amorphous transition. The temperature dependence of elastic moduli for the La- and Ce-based REBMGs is shown in Fig. 16(b) and (c). On decreasing T, the elastic moduli of $La_{68}Al_{10}Cu_{20}Co_2$ increase monotonically (smaller variation of K than those of G and E) indicating that the continuous stiffness of the REBMG is similar to that of the Mg-, Cu-, Zr-based BMGs. For the Ce-based REBMG, the E and G display stiffening modes with decreasing temperature just like other BMGs, whereas the K abnormally decreases with decreasing temperature indicating a remarkable softening behavior. The abnormal behavior of

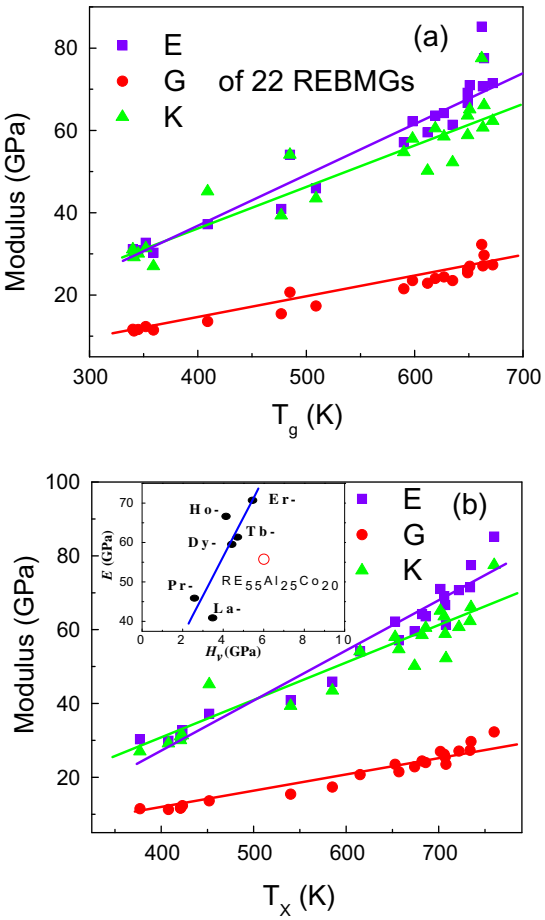

Fig. 14. The relationship between K, G, E, and T_g, T_x of typical 22 REBMGs. Data are collected from Tables 2–4. The inset of (b) shows the correlation of Vicker's hardness H_v and E for $RE_{55}Al_{25}Co_{20}$. The solid lines are guides for eyes.

Ce-based REBMG is attributed to the special local structure, especially the alterative valences and unstable electronic configurations of Ce. Since the energy levels of the inner 4*f* electrons of Ce element are so closed to those of the outer or valence 5*d* and 6*s* levels, only small amounts of energy are necessary to change the relative occupancy of these electronic levels. It has been found that the valence of Ce becomes a non-integral valence 3.67 below 100 K comparing the 3 at RT, which corresponds to the lattice collapse arising from the change in electronic structure. Accordingly, the softening of longitudinal acoustic phonons and the sharp drop of bulk modulus of the Ce-based REBMGs, can be ascribed to the relaxed structure and the shrinkage of atomic radius owing to the continuous increased valence of Ce upon cooling; and the larger volume shrinkage has been proved [124].

Experimentally distinguishable responses of acoustic and elastic properties to pressure for different kinds of glasses are observed, which suggests that the short or intermediate range ordered local structure determines the elastic and many other properties of various glasses [95,104,126–129]. Fig. 17 shows pressure dependences of V_L and V_T for typical BMGs and the non-metallic glasses at RT, all of which exhibit a nearly linear relation to pressure indicating the elastic response up to 0.5 GPa. The Nd-based REBMG shares the similar behaviors with that of typical Zr- and Pd-based BMGs, all the velocities of which increase with increasing pressure. And the change of V_L upon pressure is larger that of V_T, indicating that longitudinal phonon mode is more sensitive to pressure at least up to 0.5 GPa. Surprisingly, the Ce-based

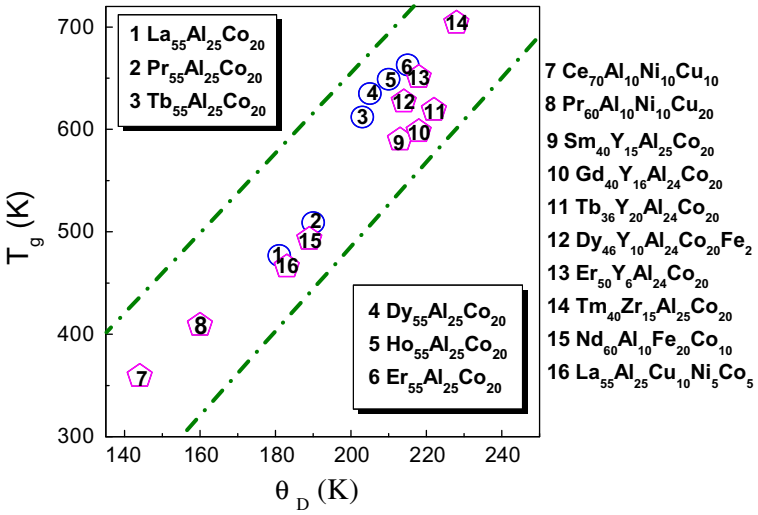

Fig. 15. The relation between T_g and Debye temperature θ_D for typical REBMGs. The dashed lines are guides for eyes.

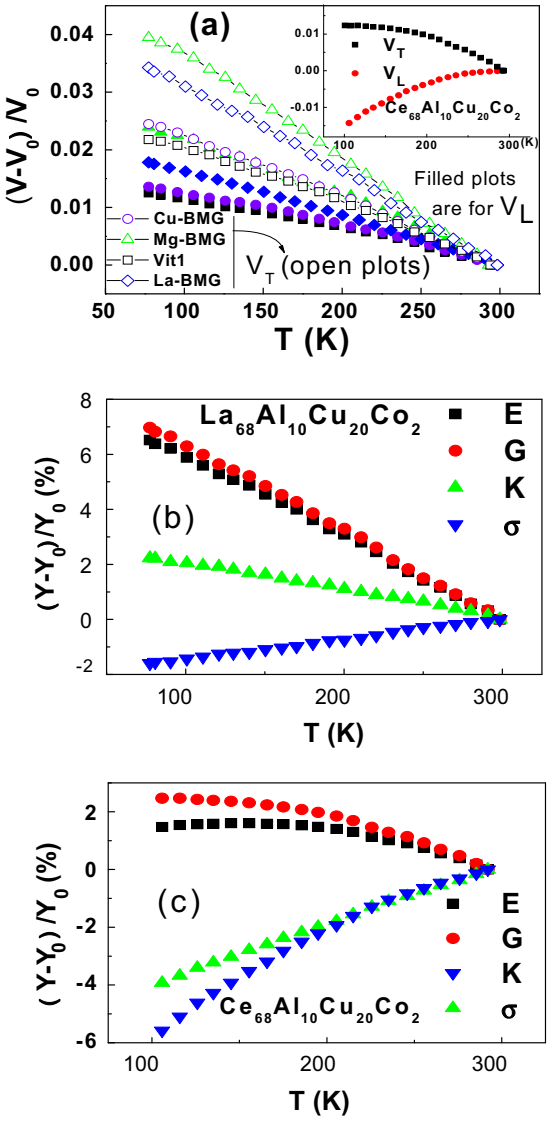

Fig. 16. (a) Varition of acoustic velocity with temperature for Vit1, $(Cu_{50}Zr_{50})_{95}Al_5$, $La_{68}Al_{10}Cu_{20}Co_2$, $Ce_{68}Al_{10}Cu_{20}Co_2$ and $Mg_{65}Cu_{25}Gd_{10}$. (b, c) Varition of the elastic moduli with temperature for $La_{68}Al_{10}Cu_{20}Co_2$ and $Ce_{68}Al_{10}Cu_{20}Co_2$.

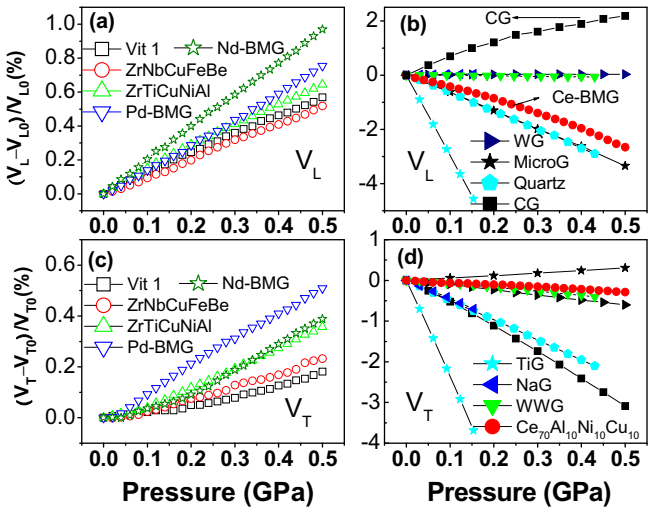

Fig. 17. Pressure dependences of V_L and V_T for $Zr_{41}Ti_{14}Cu_{12.5}Ni_{10.2}Be_{22.5}$ (Vit1), $Ce_{70}Al_{10}Ni_{10}Cu_{10}$, $Zr_{48}Nb_8Cu_{12}Fe_8Be_{24}$, $Zr_{50.6}Ti_{5.2}Cu_{18.8}Ni_{14.1}Al_{14.3}$, $Nd_{60}Al_{10}Fe_{20}Co_{10}$, $Pd_{39}Ni_{10}Cu_{30}P_{21}$, amorphous carbon (CG) and oxide glasses. The oxide glasses are window glass (WG), water white glass (WWG), fused quartz (Quartz), floats glass (NaG) and $SiO_2 + TiO_2$ glass (TiG).

REBMG has a negative pressure dependence of acoustic velocities just like most nonmetallic glasses, such as fused quartz, float glass (NaG) and water white glass (WWG). These non-metallic glasses have markedly different structure from other BMGs. Note that the decrease of V_L is about 20 times larger than that of V_T for the Ce-based REBMG, suggesting a much softer longitudinal phonon mode under pressure. These experiments suggest the unique electric and atomic structure of Ce-based alloys among BMGs families, and some similar microstructure existing between the Ce-based REBMGs and the covalent bonded oxide glasses. This can be further exhibited in the response of elastic properties to pressure.

Fig. 18(a) presents pressure dependence of G, K, and σ for two REBMGs and a Zr-based BMG. For all the BMGs the relative change of K upon pressure is larger than those of G and E. Different from the Zr- and Nd-based BMGs, all the elastic moduli of which increase with pressure as a consequence of vibrational anharmonicity, the K and σ of the Ce-based REBMG exhibit the largest decreases up to −6.1% and −3.9% at a pressure change of 0.5 GPa,

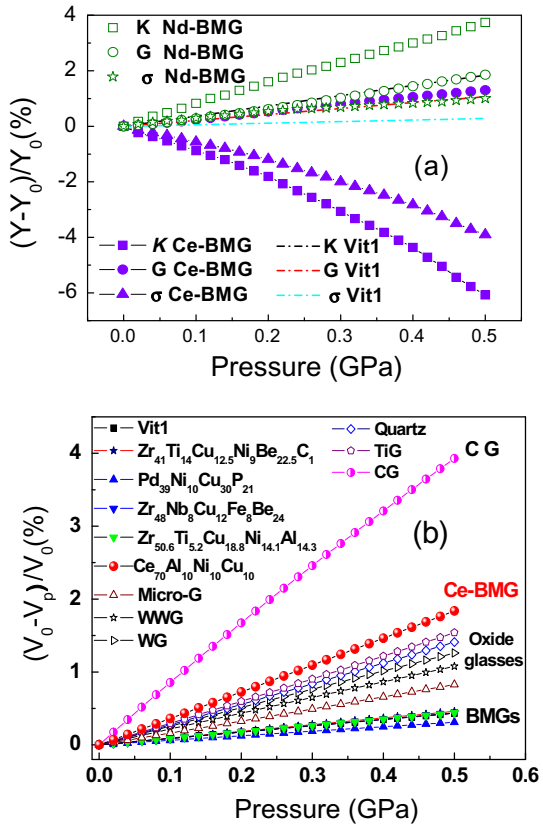

Fig. 18. (a) Comparison of the relative variations of G, K and σ with pressure up to 0.5 GPa for $Ce_{70}Al_{10}Ni_{10}Cu_{10}$, $Nd_{60}Al_{10}Fe_{20}Co_{10}$ and Vit1 at RT. (b) The EOS of $Ce_{70}Al_{10}Ni_{10}Cu_{10}$, other BMGs, oxide glasses and amorphous carbon (CG).

respectively. The Poisson ratio, σ, remains nearly constant or shows small variations in the Nd-, Zr-, Cu-, and Pd-based BMGs. However, the large variations of σ, K and ρ under pressure reveal a large pressure-induced structure change of the Ce-based REBMG. Possible amorphous to amorphous transition may be speculated at higher pressure. Fig. 19 shows the pressure-induced variations $\Delta Y(p)/Y(p_0)$ for typical BMGs, oxide glasses and amorphous carbon, from which the similarity between the Ce-based REBMG and oxide glasses is impressive. Based on the K and its pressure dependence,

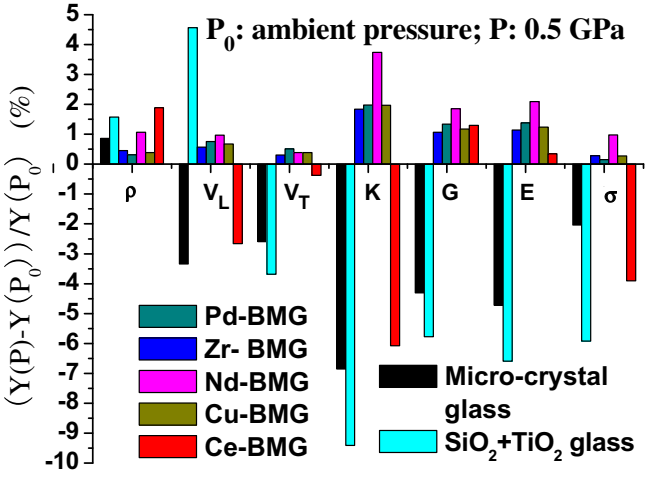

Fig. 19. Relative pressure-induced variations of ρ, V_L, V_T, G, K and σ for REBMGs and oxide glasses.

the isothermal equation of state can be established according to the Murnaghan equation [130]. Typical volume compression of various glasses is shown in Fig. 18(b), from which it can be seen that compressibility of the Ce-based REBMG is again close to that of silicate glasses than other BMGs. Note that the compression curves of the BMG lies among those of its metallic components and is nearly an average of those of its elements. This is in accord with the correlation of the modulus of the BMGs with their constituents at ambient pressure. Since the compressibility of a solid is determined by the nature of the interatomic potential and the atomic configuration, the good relationships of the compression of BMGs with its components imply that the highly packed short-range order structure of BMG has close correlation with the local atom configurations in their metallic components.

Until now it is not clear whether polyamorphism is a general feature of amorphous materials with various short-range order structures, and how the polyamorphism depends on the bonding feature of constituent atoms. Usually, the amorphous solids showing polyamophism are these systems which have directional or open coordination environments such as amorphous ice, silica, silicon and chalcogenide glasses [131–137]. Despite of different bonding characters of these materials, they share a trait that their constituent atoms have preferred bonding geometries. Until recently it has been realized that the preferred bonding characteristic is not necessary for polyamorphism (though certainly favoring it), since the polyamorphism has been observed in a Ce-based metallic glass ribbon with non-directional metallic bonding feature, different from the network-forming glasses [138]. This is just like crystalline Ce, which exhibits polymorphic transitions from γ-f.c.c. to α-f.c.c. structure starting from rather low pressures of about 1 GPa [139], the transformation of the low density state to the high density state is ascribed to the interaction of strongly correlated 4f electrons and their delocalization under pressure resulting in bond shortening, as pointed out by the authors.

Our work about the Ce-based REBMG indicates an anomalous soft behavior both in longitudinal and transverse acoustic modes under pressure similar to that of typical oxide glasses, indeed suggesting a significant structural change (or underlying transformation) under pressure [129]. Interestingly, at low temperature some anomalous behaviors in the elastic properties are also observed in the Ce-based REBMGs, indicating that the possible polyamorphism can even be induced by temperature [124]. In a La–Ce-based REBMG, Zeng et al. has found an unusual change in the compressibility at ~14 GPa, a behavior suggestive of polyamorphism in this alloy [140]. And the possible amorphous to amorphous transition has also been suggested in the La- and Nd-based REBMGs from the electric resistance behavior under pressure [141]. Detailed explorations of the behaviors of BMGs under extreme conditions such as high pressure, low temperature and high magnetic filed are highly required, to check the conditions under which polyamorphism is or not manifested.

3.5. Spin dynamics of REBMGs

In the last several decades, the original type of spin-glass (SG) materials such as AuFe, AgMn and CuMn, has been extended to include a large number of so-called SG like materials such as surface SG, reentrant SG, cluster SG and random magnetic systems [142–154]. These materials usually bring forward new phenomenon and more complicated problems, and enrich the random and complex system field. The impact of random magnetic anisotropy (RMA) and clusters contained inhomogeneous structure on the spin dynamics are unclear [149–160]. For magnetic nanoparticles it is proposed that heterogeneities such as dispersion in the particle size distribution would inhibit the critical character of transition. However, a highly heterogeneous nanogranular system has

been shown to exhibit critical dynamics in its transition to a low temperature spin-glass-like phase [161]. At present it is blurry whether inhomogeneous structure from multi-phases can inhibit the critical dynamics and whether the multiple SG like phases can coexist, since the most conventional SG materials contain only one SG phase, or coexistence with a ferromagnetic (antiferromagnetic) phase. Accordingly, a sample with intrinsic multiple SG transitions is highly desirable and since it is closely associated with the prototype of multiple complex systems. Such a model system has been investigated in a $Pr_{60}Al_{10}Ni_{10}Cu_{16}Fe_4$ REBMG [16]. This unusual behavior is ascribed to the coupling of magnetic nanoclusters and amorphous matrix. Another factor that distinguishes REBMGs from the conventional SG is the random single ion magnetic anisotropy interaction which can be competitive to, and even dominate over, the exchange interaction J, especially in Nd-, Tb-, Ho- and Dy-based REBMGs. In SG, the random exchange interaction plays the dominant role, and only slight anisotropy D ($\gg J$) exits which plays a subtle role in the nature of transition [155,156]. In the strong RMA limit for $D/J \gg 1$, it usually is described as speromagnetic (SM) state [150–152]. Theoretical works show that in $D \to \infty$ case the RMA possesses the Ising spin-glass (ISG) behavior [159,160]. However, the evidence for directly relating energy structure and critical slow dynamics of a strong RMA system to an ISG is not conclusive. The nature of RMA system and the correlation with SG are still unsettled questions.

3.5.1. Muti spin-glass behavior of Pr-based REBMGs

Fig. 20 shows the zero field cooled (ZFC) and field cooled (FC) magnetization of $Pr_{60}Al_{10}Ni_{10}Cu_{16}Fe_4$ REBMG. A cusp in ZFC curve and the onset of the irreversibility between the ZFC and FC curves around 14 K are typical SG features. A careful analysis of the ZFC and FC branches clearly reveals the coexistence of another slight irreversibility between the ZFC and FC curves around $T_{F3} \approx 250$ K. A sudden increase in the FC magnetization below $T_{F1} \approx 8$ K can be seen in the inset of Fig. 20. It is noted that the irreversible magnetization near RT is two orders of magnitude lower than that around T_{F2} and the peak is rather broad, indicating some spin clusters are frozen instead of single spin. The coexistence of three different SG phases has also been confirmed by the temperature dependent *ac* susceptibility. From Fig. 21, it can be seen that all the χ' curves show two maxima at $T_{F2} \sim 14$ K and $T_{F3} \sim 280$ K, and a small shoulder around $T_{F1} \sim 6$ K; whereas the χ'' curves show three well-defined peaks near T_{F1}, T_{F2}, and T_{F3}. All the amplitude and position of the peaks or shoulders depend on frequency. The value of the frequency sensibility at T_{F1}, T_{F2}, and T_{F3}, are determined to be 0.005, 0.012, and 0.01, respectively, falling into the typical values of SGs. The frequency dependences of these freezing temperatures are all fitted by the Vogel–Fulcher formula: $\omega = \omega_0 \exp[-E_a/k_B(T_F - T_0)]$. The best fitting values are $\omega_{01} \approx 10^{13}$ Hz, $E_{a1} \approx 31$ K and $T_{01} = 4.5$ K; $\omega_{02} \approx 10^{13}$ Hz, $E_{a2} \approx 40$ K and $T_{02} = 12.6$ K; $\omega_{03} \approx 10^{7}$ Hz, $E_{a3} \approx 275$ K and $T_{03} = 233$ K. Compared with the value of $\omega_{03} \approx 10^{7}$, ω_{01} and ω_{02} (both $\sim 10^{13}$ Hz, just as most SG systems) are much larger, which suggests a slower spin dynamics near RT associated with the relaxation of large spin clusters. The multiple SG like feature is further confirmed by the electric transport property and the glass dynamics [16].

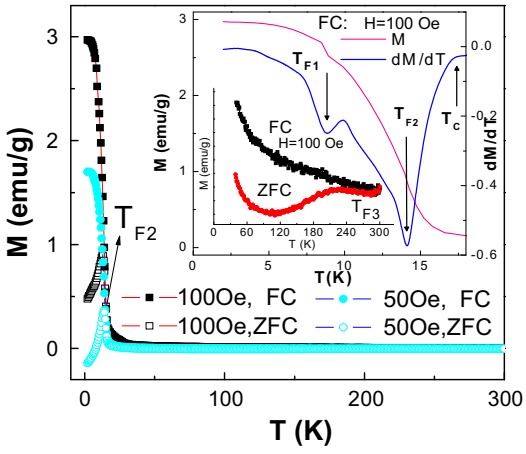

Fig. 20. FC and ZFC magnetization measured at 100 Oe and 50 Oe for a Pr-based BMG. The inset shows typical FC curve M (left axis) and dM/dT (right axis) measured at 100 Oe. The enlarged FC and ZFC branches in high temperature are also shown in the inset [16].

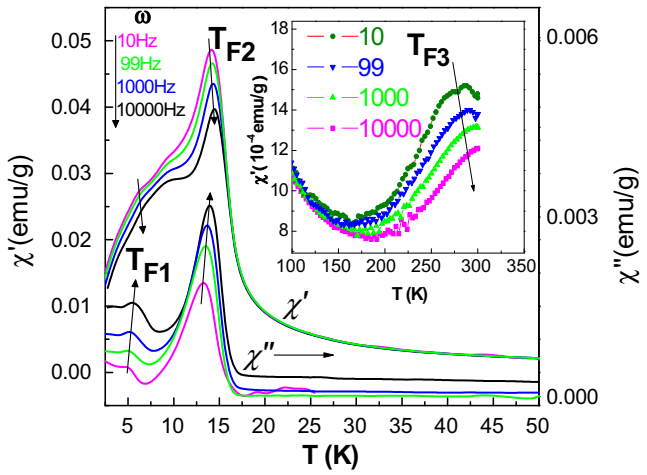

Fig. 21. Real (χ') and imaginary (χ'') components of the ac susceptibility at frequencies from 10 Hz to 10 kHz in an applied ac field of 10 Oe. The inset shows the *ac* susceptibility in high temperature [16].

The multiple SG like behaviors are associated with the inhomogeneous microstructure of the Pr-based REBMG. Although typical amorphous structure is suggested in the XRD pattern, detailed structure information from magnetic-force microscope and HTEM indicate some nanoclusters embedded in the amorphous matrix [16]. The intrinsic inhomogeneity partially arises from the positive heat of mixing between Pr and Fe, which makes the liquid structure less stable and facilitates nano-scale nucleation in the SL state. Accordingly, the cluster SG freezing at $T_{F3} \sim 280$ K can be ascribed to the ferromagnetic Fe (Ni) contained nanoclusters. The paramagnetic Pr-based amorphous matrix and Pr nanoclusters contribute to the reentrant SG at $T_{F2} \sim 14$ K, and the cluster SG at $T_{F1} \sim 6$ K. Therefore, the Pr-based REBMGs with different SG phases thus provide an ideal prototype for understanding practical more complex systems since most technologically relevant magnetic materials are composed of two phases (or more) with different magnetic properties on nanometers scale [16].

3.5.2. Spin dynamics with strong random magnetic anisotropy

Although it has been long established that the long range order in RMA is broken, the ground state and the critical dynamics are complicated and obscure due to the disordered structure and the competition between D and J. These questions have partly been addressed recently in $Dy_{40}Al_{24}Co_{20}Y_{11}Zr_5$ REBMG exhibiting strong RMA [162]. From the critical and slow dynamics it has been found that there are agreement in some aspects between theoretical simulations of ISG (and RMA) and experimental results, but also significant quantitative differences exist.

It is known that for ISG an Almeida–Thouless (A–T) line [163] is theoretically predicted as a transition line in magnetic field and has

been experimentally observed for many SGs. From the ZFC and FC measurements of the Dy-based REBMG, a transition line in the form of A–T line has been obtained in the low field regime suggesting the ISG like property as shown in Fig. 22. However, a crossover behavior occurs in high field (above ~4000 Oe) region which may associate with HSG like behavior. Similar HSG to ISG crossover has been predicted by Kotliar and Sompolinsky [164] in a mean-field model of a HSG with weak random Dzyaloshinsky–Moriya anisotropy. Despite $D \gg J$, anisotropy can mix the longitudinal and transverse spin components resulting only an A–T transition line in low field limit like an ISG, and higher field recovers HSG nature. In term of the above results, it is possible to conclude that some common characters exist among real HSG, ISG and strong RMA in the low field limit. Fig. 23 displays the characteristic of *ac* susceptibility for the alloy [162]. It is clearly that the susceptibility of 10 Oe superposes on the curve of 0.1 Oe in the whole temperature range suggesting the linear response to the filed perturbation. And the relationship $\chi''(\omega) = \frac{\pi}{2}\frac{d\chi'(\omega)}{d\ln\omega}\chi'$ is precisely obeyed for the whole temperature range measured at both 33 Hz and 6666 Hz as shown in Fig. 23(b), indicating the broad distribution of relaxation time. Furthermore, the relaxation of low field *ac* susceptibility above T_g, reflecting the dynamic spin-correlation function $q(t)$, is found to be successfully analyzed using an equation similar to the Ogielski function [165] obtained in MC simulations on a short-range ISG. These features suggest the similarity of RMA and ISG especially in the low field region.

However, the large random anisotropy has an important impact on the spin dynamics distinguishing the strong RMA from ISG in the following ways: first, it slows the relaxation of spins in the critical range near T_g reflecting in the larger characteristic relaxation time $\sim 10^{-6}$ s compared with typical $\sim 10^{-10}$–10^{-13} s for SG. Second, it shows slower aging dynamics below T_g and the time dependent phenomenon is characterized by a power law times a stretched exponential functional form, which deviates from the simulation results of Ogielski and that of some ISGs reported both showing algebraic dependence behavior [162]. Thirdly, after cooling in a magnetic field, the spin is in favor of the field direction, and this 'frozen' initial magnetization can be 'pinned' by the strong RMA resulting in a vertical shift of the magnetic hysteresis loop in certain fields range (Fig. 22(d)). These results indicate that the strong RMA can belong to a different universality class from the (Ising) SG, although several common features are shared between them.

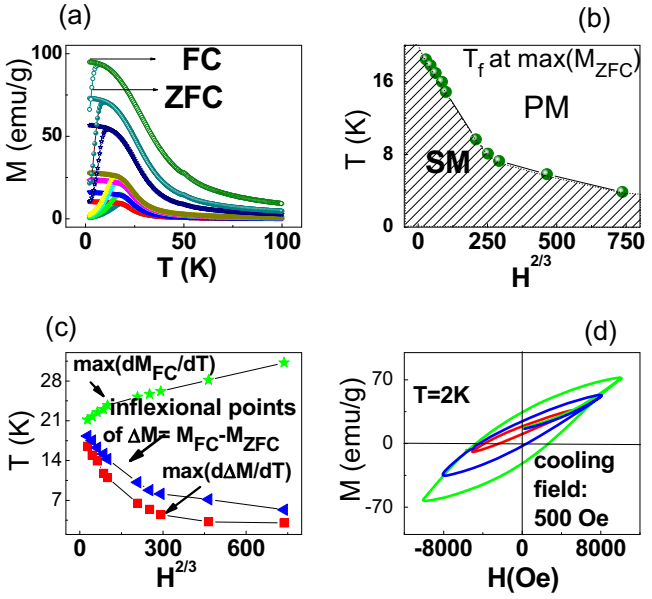

Fig. 22. (a) Temperature dependence of the ZFC and FC magnetization of $Dy_{40}Al_{24}Co_{20}Y_{11}Zr_5$. (b) Field dependence of T_f. (c) Field dependence of other characteristic temperatures. (d) Magnetic hysteresis loop at 2 K after field of 500 Oe cooling between ±5080, ±8080 and ±10080 Oe [162].

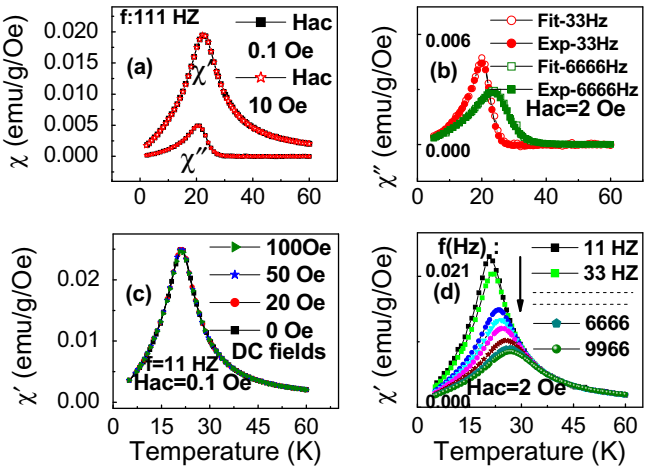

Fig. 23. (a) The χ' at 111 Hz with different probing *ac* filed. (b) χ'' got from experiment directly compared with obtained from Lendgren relation under an *ac* magnetic field of 2 Oe. (c) The χ' under different DC fields. (d) The χ' at frequencies ranging from 10 to 10^4 Hz [162].

3.6. Electric properties of REBMGs

In the 1960s–1980s there are considerable efforts and progress on the fundamental understanding of the electric, magnetic and other low temperature transport behaviors of metallic glasses [1,114]. However, the understandings of the electric and magnetic structure of metallic glass are far from being adequately solved owing to the complex structure and limited dimension of the ribbon. The BMGs facilitate the investigation not only on the mechanical properties, but also the electric properties, and in particular their correlations. Thus, a deeper understanding of the atomic and electronic configuration of metallic glasses is now possible by combining the electric, elastic and mechanical explorations. The lanthanides characterize themselves by their narrow 4*f* electronic structure (for La the 4*f* shell is empty) which bring about a profuse magnetic and electric properties of REBMGs, such as the superconductivity of La-based REBMGs, hard magnetism of Nd(Pr)-based REBMGs mentioned above and the heavy fermion behavior of Ce-based REBMGs.

3.6.1. Superconductivity of La-based REBMGs

Superconductivity in La-based REBGM has been reported [166]. The density of states at the Fermi level, the electron–phonon interaction parameter λ, and the Debye temperature of the REBMG are determined to be 1.75 eV^{-1} at^{-1}, 0.68, and 122 K, respectively. The amplitude of λ indicates that this alloy is an intermediate coupling superconductor. It is noted that the λ of La-based REBMG is larger than that of a Zr-based BMG (~0.49). And both alloys distinguish themselves from the non-transition-metal amorphous alloys which have been identified as strong-coupling superconductors with λ in the vicinity of 2. A comparison of the superconductivity between the Zr-based BMG and its crystalline counterpart reveals the following differences [167]: firstly the BMG shows negative temperature coefficients of the resistivity between about 4.2 and 300 K, whereas the crystallized sample shows positive temperature coefficients; secondly at zero magnetic field the transition width of the crystallized alloy is broadened compared with that

of the as cast sample. This broadness may be ascribed to the smearing of the density of states associated with the short mean free path in the disordered alloys. Interestingly, due to its sensitivity to the electronic and atom structure, the resistivity in the normal state of La-based REBMGs and other BMG families can be used to monitor the structure evolution during relaxation, glass transition and crystallization, and even evaluate the glass-forming ability [168–174].

3.6.2. Heavy fermion behavior of Ce-based REBMGs

Heavy fermion (HF) systems characterized by electrons with extremely large effective masses. Many fascinating properties occur in these systems as a consequence of the competition between the local Kondo resonance and magnetic ordering [175–177]. The corresponding heavy-electron 'quasiparticle' states are close to the Fermi energy and govern the thermodynamic, electric and magnetic properties of these materials. For the case of RE compounds, it is extensive debated whether it is sufficient to treat the *f* states as localized impurities (single-impurity Anderson model) or whether the periodic crystal symmetry must be considered (periodic Anderson model). Furthermore, it has been recognized that the HF behavior is strongly affected by disorder due to alloying, lattice defects, etc., which has obtained evidences both from the dynamical mean-field theory and experimental data [178–183]. However, it is still not clear the interplay between the degree of disorder and strong correlations behavior in HF materials, since only weak disorder exists in intermetallic materials and theoretical models.

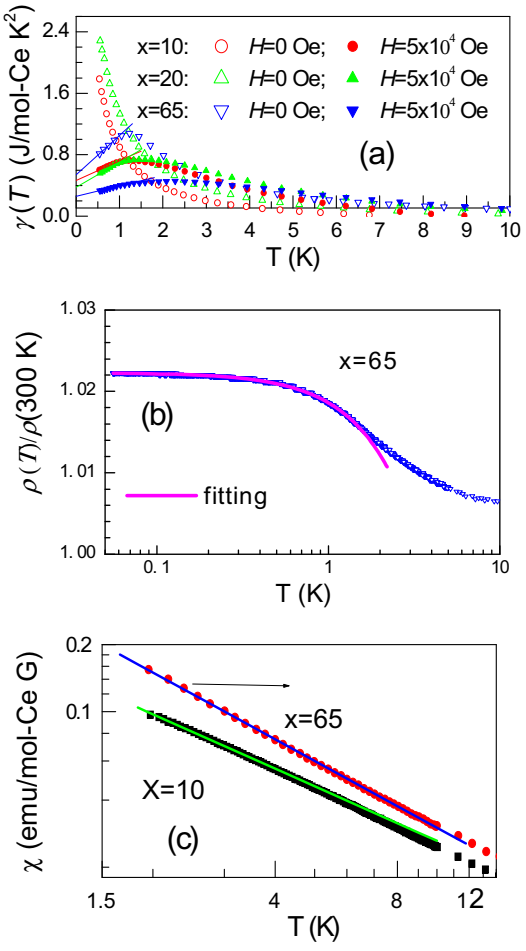

Fig. 24. (a) The $\gamma(T)$ vs T of the REBMGs at $H = 0$ and 5×10^4 Oe $Ce_x La_{65-x} Al_{10} Cu_{20} Co_5$ REBMGs ($x = 0$, 10, 20, and 65). (b) The T-dependent ρ of the BMG ($x = 65$). The solid line denotes the fitting result of the BMG ($x = 65$) by $\rho = \rho_0 + AT^n$, with $n = 1.454$. (c) The *dc* magnetic susceptibility χ for the $Ce_x La_{1-x} Al_{10} Cu_{20} Co_5$ ($x = 10$ and 65) REBMGs at low T. The solid line is the fitting with $\chi \propto T^{-1+\lambda}$. The straight red line denotes the linear extrapolation [44]. (For interpretation of the references in colour in this figure legend, the reader is referred to the web version of this article.)

Recently, remarkable HF behaviors has been observed in the $Ce_x La_{65-x} Al_{10} Cu_{20} Co_5$ REBMGs ($x = 0$, 10, 20, and 65 at.%) [44]. Direct evidence suggesting the HF characteristic is from the heat capacity of these alloys. From the contribution of the 4*f* electrons to heat capacity, the linear coefficients γ (C_{el}/T) at 0.53 K for the REBMGs with $x = 10$, 20, and 65 are 1789, 2282, and 811 mJ/mol-Ce K^2, respectively, indicating the HF feature (Fig. 24(a)). The change of the low T properties with Ce content is due to the competition between the Kondo effect and the RKKY interaction [175–179], which is tuned by the average distance between Ce atoms. And the HF behavior can also be tuned by the magnetic field. The γ (0 K) decreases with increasing annealing time below T_g (which induces the structure ordering), indicating that electric correlations relate closely to the disordered structure of the glass. In accordance with the theory prediction that sufficient disorder can result in a breakdown of conventional Fermi-liquid behavior, these REBMGs exhibit non-Fermi-liquid features (see Fig. 24(b–d)) as indicated from the dependence of χ on $T^{-1+\lambda}$ (with $y = 0.187$ for $x = 10$) and the dependence of the resistivity ρ on T^n ($n = 1.454$) at low temperature [184,185].

The influence of disordered structure on the competition between the Kondo resonance and magnetic ordering has been studied. For Ce compounds, when the *f* level of Ce is right at E_F, strong Kondo resonance overrides the RKKY interaction; when it is far above or below E_F, the local Kondo resonance is weak and the RKKY interaction dominates. That is in the crossover region where the HF happens. Ascribed to the amorphous structure, the distributed *f* levels and the Fermi level within the band of *f* levels of the Ce-based REBMGs, produce a wide range of strengths of the Kondo resonance and the coexistence of atomic sites in the valence fluctuation regime, the spin-glass sites dominated by the RKKY interaction, and the crossover sites that show the HF behavior. Accordingly, the reduction of γ by isothermal annealing can be understood by the structure relaxation inducing narrower *f* levels. The smaller γ for $x = 65$ compared with other three means that most of the *f* levels sink well below E_F and reduce the HF effect. The detailed mechanism of the HF of these REBMGs remains a challenge.

4. Summary

A series of REBMGs were developed and attracted intense research interest in the last decade. The main commercial prospects of the REBMGs lie in their high-performance in applications as promising micro-structures, hard magnets and magnetic refrigerants and so on. With the development of new systems and the discovery of more unique properties, broader application, including their use as magnetic recording/storage and magnetostriction materials, could be expected in the future. The application of metallic glasses as functional materials can also avoid some common flaws of the materials such as brittleness, cost and limited glass-forming ability. The great advantage for the applications of these REBMGs are that they can be produced using a one-step process in to different shapes (such as spheres, balls, thin sheets or plates, wires, rings, rods and others). There is also increased freedom to tailor the electric, mechanical and magnetic properties owing to the flexibility in composition, shape and dimensions of the new metallic glasses. The 'elastic modulus rule' can guide the search for new REBMGs with good GFA, and controlled/desired

properties. From a fundamental perspective, the REBMGs exhibit profuse and versatile physical properties, such as low temperature thermoplastic, spin freezing dynamics, hard magnetism, HF behavior and polymorphism, all of which offer more challenges and opportunities for glass science.

Acknowledgements

The authors are indebted to the experimental assistances and discussions from Professor M.X. Pan, D.Q. Zhao, Professor R.J. Wang, Professor H.Y. Bai, Professor B.C. Wei, Dr L. Xia, Dr P. Wen, Dr M.B. Tang, Dr S. Li, Dr Y.X. Wei, Dr Yong Li, Dr B. Zhang, Dr Z.F. Zhao, Dr P. Yu, Dr T.Y. Wang, X.F. Liu, J.Q. Wang, J.G. Wang, J.F. Li, X.X. Xia, K. Zhao, H.B. Yu, and B.A. Sun. Financial supports from the National Natural Science Foundation of China (Nos. 50621061 and 50731008) and MOST 973 (No. 2007CB613904) are acknowledged.

References

[1] [a] H.S. Chen, Rep. Prog. Phys. 43 (1980) 353;
[b] J.H. Li, X.D. Dai, S.H. Liang, K.P. Tai, Y. Kong, B.X. Liu, Phys. Rep. 455 (2008) 1;
[c] B.X. Liu, W.S. Lai, Q. Zhang, Mater. Sci. Eng. R 29 (2000) 1.
[2] A. Inoue, T. Zhang, T. Masumoto, Mater. Trans. JIM 30 (1989) 965.
[3] W.H. Wang, Prog. Mater. Sci. 52 (2007) 540.
[4] A. Inoue, Acta Mater. 48 (2000) 279.
[5] [a] W.H. Wang, C. Dong, C.H. Shek, Mater. Sci. Eng. R 44 (2004) 45;
[b] M.B. Tang, D.Q. Zhao, M.X. Pan, W.H. Wang, Chin. Phys. Lett. 21 (2004) 901;
[c] W.H. Wang, J.J. Lewandowski, A.L. Greer, J. Mater. Res. 20 (2005) 2307;
[d] W.H. Wang, Z.X. Bao, J. Eckert, Phys. Rev. B 61 (2000) 3166;
[e] W.H. Wang, Q. Wei, S. Friedrich, Phys. Rev. B 57 (1998) 8211;
[f] W.H. Wang, D.Q. Zhao, D.W. He, Y.S. Yao, Appl. Phys. Lett. 75 (1999) 2770;
[g] Y.D. Dong, W.H. Wang, K.Q. Xiao, L. Liu, S.H. Tong, Y.Z. He, Mater. Sci. Eng. A 134 (1991) 867.
[6] A. Inoue, A. Kato, T. Zhang, S.G. Kim, T. Masumoto, Mater. Trans. JIM 32 (1991) 609.
[7] T. Zhang, A. Inoue, T. Masumoto, Mater. Trans. JIM 32 (1991) 1005.
[8] A. Peker, W.L. Johnson, Appl. Phys. Lett. 63 (1993) 2342.
[9] A. Inoue, K.T. Zhang, W. Zhang, A. Takeuchi, Mater. Trans. JIM 37 (1996) 99.
[10] L.Q. Xing, J. Eckert, W. Löser, S. Roth, L. Schultz, J. Appl. Phys. 88 (2000) 3565.
[11] G.J. Fan, W. Löser, S. Roth, J. Eckert, L. Schultz, Appl. Phys. Lett. 75 (1999) 2984.
[12] J. Ding, Y. Li, X.Z. Wang, J. Phys. D 32 (1999) 713.
[13] [a] B.C. Wei, W.H. Wang, D.Q. Zhao, Y. Zhang, M.X. Pan, B.S. Han, Z.R. Zhang, W.R. Hu, Phys. Rev. B 64 (2001) 012406;
[b] B.C. Wei, Y. Zhang, Y.X. Zhuang, D.Q. Zhao, M.X. Pan, W.H. Wang, J. Appl. Phys. 89 (2001) 3529.
[14] F. Guo, S.J. Poon, Appl. Phys. Lett. 83 (2003) 2575.
[15] Z.F. Zhao, Z. Zhang, W.H. Wang, Appl. Phys. Lett. 82 (2003) 4699.
[16] Y.T. Wang, H.Y. Bai, M.X. Pan, D.Q. Zhao, W.H. Wang, Phys. Rev. B. 74 (2006) 064422.
[17] B. Zhang, M.X. Pan, D.Q. Zhao, W.H. Wang, Appl. Phys. Lett. 85 (2004) 61.
[18] B. Zhang, W.H. Wang, Phys. Rev. B 70 (2004) 224208.
[19] B. Zhang, M.X. Pan, D.Q. Zhao, W.H. Wang, Phys. Rev. B 73 (2006) 092201.
[20] B. Zhang, D.Q. Zhao, M.X. Pan, R.J. Wang, W.H. Wang, Acta Mater. 54 (2006) 3025.
[21] S. Li, R.J. Wang, M.X. Pan, D.Q. Zhao, W.H. Wang, Scr. Mater. 53 (2005) 1489.
[22] S. Li, R.J. Wang, M.X. Pan, D.Q. Zhao, W.H. Wang, Intermetallics 14 (2006) 592.
[23] S. Li, D.Q. Zhao, M.X. Pan, W.H. Wang, J. Non-Cryst. Solids 351 (2005) 2568.
[24] S. Li, X.K. Xi, Y.X. Wei, Q. Luo, Y.T. Wang, M.B. Tang, B. Zhang, Z.F. Zhao, R.J. Wang, M.X. Pan, D.Q. Zhao, W.H. Wang, Sci. Technol. Adv. Mater. 6 (2005) 823.
[25] S. Li, R.J. Wang, M.X. Pan, D.Q. Zhao, W.H. Wang, J. Non-Cryst. Solids 354 (2008) 1080.
[26] [a] X.K. Xi, S. Li, R.J. Wang, M.X. Pan, D.Q. Zhao, W.H. Wang, J. Mater. Res. 20 (2005) 2243;
[b] X.K. Xi, D.Q. Zhao, M.X. Pan, W.H. Wang, J. Non-Cryst. Solids 344 (2004) 105.
[27] Y.X. Wei, M.X. Pan, W.H. Wang, Scr. Mater. 54 (2006) 599.
[28] Q. Luo, D.Q. Zhao, M.X. Pan, R.J. Wang, W.H. Wang, Appl. Phys. Lett. 88 (2006) 181909.
[29] [a] H.B. Yu, P. Yu, W.H. Wang, H.Y. Bai, Appl. Phys. Lett. 92 (2008) 141906;
[b] J.Q. Wang, W.H. Wang, H.Y. Bai, Appl. Phys. Lett. 94 (2009) 041910;
[c] J.F. Li, D.Q. Zhao, M.L. Zhang, W.H. Wang, Appl. Phys. Lett. 93 (2008) 171907.
[30] Y.T. Wang, Z.Y. Pang, R.J. Wang, D.Q. Zhao, M.X. Pan, B.S. Han, W.L. Wang, W.H. Wang, J. Non-Cryst. Solids 352 (2006) 444.
[31] Z.F. Zhao, P. Wen, W.H. Wang, J. Mater. Res. 21 (2006) 369.
[32] Z. Li, H.Y. Bai, M.X. Pan, D.Q. Zhao, W.L. Wang, W.H. Wang, J. Mater. Res. 18 (2003) 2208.
[33] Z. Zhang, D.Q. Zhao, W.H. Wang, J. Mater. Res. 20 (2005) 314.
[34] L. Xia, M.B. Tang, H. Xu, M.X. Pan, D.Q. Zhao, W.H. Wang, Y.D. Dong, J. Mater. Res. 19 (2004) 1307.
[35] X.F. Liu, R.J. Wang, D.Q. Zhao, M.X. Pan, W.H. Wang, Appl. Phys. Lett. 91 (2007) 041901.
[36] Y.T. Wang, X.X. Kui, Y.K. Fang, D.Q. Zhao, M.X. Pan, B.S. Han, W.H. Wang, Appl. Phys. Lett. 85 (2004) 5989.
[37] J.P. Chu, C.L. Chiang, H. Wijaya, R.T. Huang, C.W. Wu, B. Zhang, W.H. Wang, T.G. Nieh, Scr. Mater. 55 (2006) 227.
[38] Z. Bian, A. Inoue, Mater. Trans. 46 (2005) 1857.
[39] D. Chen, A. Takeuchi, A. Inoue, Mater. Sci. Eng. 457 (2007) 226.
[40] B.C. Wei, W. Löser, W.H. Wang, J. Eckert, Acta Mater. 50 (2002) 4357.
[41] W.H. Li, Keesam Shin, B.C. Wei, Appl. Phys. Lett. 90 (2007) 171928.
[42] A.A. Kundig, T. Schweizer, E. Schaflerc, J.F. Löffler, Scr. Mater. 56 (2007) 289.
[43] Q.K. Jiang, G.Q. Zhang, L. Yang, X.D. Wang, K. Saks, H. Franz, R. Wunderlich, H. Fecht, J.Z. Jiang, Acta Mater. 55 (2007) 4409.
[44] M.B. Tang, H.Y. Bai, W.H. Wang, D. Bogdanov, K. Winzer, K. Samwer, T. Egami, Phys. Rev. B 75 (2007) 172201.
[45] B. Zhang, D.Q. Zhao, M.X. Pan, W.H. Wang, A.L. Greer, Phys. Rev. Lett. 94 (2005) 205502.
[46] [a] Q. Luo, D.Q. Zhao, M.X. Pan, W.H. Wang, Appl. Phys. Lett. 89 (2006) 081914;
[b] Y.T. Wang, H.Y. Bai, M.X. Pan, D.Q. Zhao, W.H. Wang, Sci. China G 51 (2008) 337.
[47] Q. Luo, D.Q. Zhao, M.X. Pan, W.H. Wang, Appl. Phys. Lett. 90 (2007) 211903.
[48] D. Turnbull, Contemp. Phys. 10 (1969) 437.
[49] Z.P. Lu, C.T. Liu, Phys. Rev. Lett. 91 (2003) 115503.
[50] Y. Zhang, D.Q. Zhao, W.H. Wang, J. Non-Cryst. Solids 315 (2003) 206.
[51] F.Q. Guo, S.J. Poon, G.J. Shiflet, Scr. Mater. 43 (2000) 1089.
[52] K. Ito, C.T. Moynihan, C.A. Angell, Nature 398 (1999) 492.
[53] [a] X.K. Xi, L.L. Li, B. Zhang, W.H. Wang, Y. Wu, Phys. Rev. Lett. 99 (2007) 095501;
[b] X.K. Xi, D.Q. Zhao, M.X. Pan, W.H. Wang, Y. Wu, J.J. Lewandowski, Phys. Rev. Lett. 94 (2005) 125510;
[c] G. Wang, D.Q. Zhao, H.Y. Bai, M.X. Pan, A.L. Xia, B.S. Han, X.K. Xi, Y. Wu, W.H. Wang, Phys. Rev. Lett. 98 (2007) 235501;
[d] G. Wang, Y.T. Wang, Y.H. Liu, M.X. Pan, D.Q. Zhao, W.H. Wang, Appl. Phys. Lett. 89 (2006) 121909;
[e] X.K. Xi, D.Q. Zhao, M.X. Pan, W.H. Wang, Y. Wu, J.J. Lewandowski, Appl. Phys. Lett. 89 (2006) 181911.
[54] Q. Luo, B. Zhang, D.Q. Zhao, M.X. Pan, R.J. Wang, W.H. Wang, Appl. Phys. Lett. 88 (2006) 151915.
[55] S. Schneider, A. Bracchi, K. Samwer, M. Seibt, P. Thiyagarajan, Appl. Phys. Lett. 80 (2002) 1749.
[56] A. Bracchi, K. Samwer, S. Schneider, J.F. Löffler, Appl. Phys. Lett. 82 (2003) 721.
[57] A. Bracchi, K. Samwer, T. Niermann, M. Seibt, S. Schneider, Appl. Phys. Lett. 85 (2004) 2565.
[58] N.H. Dan, N.X. Phuc, N.M. Hong, J. Ding, D. Givord, J. Magn. Magn. Mater. 226 (2001) 1385.
[59] D. Triyono, R. Sato Turtelli, R. Grössinger, H. Michor, K.R. Pirota, M. Knobel, H. Sassik, T. Mathias, S. Höfinger, J. Fidler, J. Magn. Magn. Mater. 242–245 (2001) 1321.
[60] R. Sato Turtelli, D. Triyono, R. Grössinger, H. Michor, J.H. Espina, J.P. Sinnecker, H. Sassik, J. Eckert, G. Kumar, Z.G. Sun, G.J. Fan, Phys. Rev. B 66 (2007) 054441.
[61] A. Tsoukatos, G.C. Hadijipanayis, J. Appl. Phys. 64 (1988) 5971.
[62] D. Givord, J.P. Nozieres, M.F. Rossignol, D.W. Taylor, I.R. Harris, D. Fruchart, S. Miraglia, J. Alloys Compd. 176 (1991) L5.
[63] V.P. Menushenkov, A.S. Lileev, M.A. Oreshkin, S.A. Zhuravlev, J. Magn. Magn. Mater. 203 (1999) 149.
[64] A. Inoue, A. Takeuchi, T. Zhang, Metall. Mater. Trans. A 29A (1998) 1779.
[65] G. Kumar, J. Eckert, S. Roth, K.-H. Müller, L. Schultz, J. Alloys Compd. 348 (2003) 308.
[66] Z.G. Sun, W. Löser, J. Eckert, K.-H. Müller, L. Schultz, Appl. Phys. Lett. 80 (2002) 772.
[67] Z.G. Sun, W. Löser, J. Eckert, K.-H. Müller, L. Schultz, J. Appl. Phys. 91 (2002) 9267.
[68] R.W. McCallum, L.H. Lewis, M.J. Kramer, K.W. Dennis, J Magn. Magn. Mater. 299 (2006) 265.
[69] H.Z. Kong, Y. Li, J. Ding, J. Magn. Magn. Mater. 217 (2000) 65.
[70] V.K. Pecharsky, K.A. Gschneidner Jr., A.O. Tsokol1, Rep. Prog. Phys. 68 (2005) 1479.
[71] Z.B. Guo, Y.W. Du, H. Huang, D. Feng, Phys. Rev. Lett. 78 (1997) 1142.
[72] O. Tegus, E. Bruck, K.H.J. Buschow, F.R. deBoer, Nature 415 (2002) 150.
[73] V. Provenzano, A.J. Shapiro, R.D. Shull, Nature 429 (2004) 853.
[74] Q. Luo, Y.T. Wang, W.H. Wang, submitted for publication.
[75] T.D. Shen, R.B. Schwarz, J.Y. Coulter, J.D. Thompson, J. Appl. Phys. 91 (2002) 5240.
[76] P. Didukh, A. Ślawska-Waniewska, J. Magn. Magn. Mater. 254&255 (2003) 407.
[77] S. Atalay, H. Gencer, V.S. Kolat, J. Non-Cryst. Solids 351 (2005) 2373.
[78] S.G. Min, K.S. Kim, H.S. Suh, S.W. Lee, J. Appl. Phys. 97 (2005) 10M310.
[79] V. Franco, J.S. Blázquez, A. Conde, Appl. Phys. Lett. 88 (2006) 042505.
[80] V. Franco, J.M. Borrego, A. Conde, S. Roth, Appl. Phys. Lett. 88 (2006) 132509.

[81] K.S. Kim, S.G. Min, S.C. Yu, S.K. Oh, Y.C. Kim, K.Y. Kim, J. Magn. Magn. Mater. 304 (2006) e642.
[82] M. Foldeaki, R. Chahine, B.R. Gopal, T.K. Bose, X.Y. Liu, J.A. Barclay, J. Appl. Phys. 83 (1998) 2727.
[83] H. Fu, X.T. Zu, H.J. Yu, B.H. Teng, X.T. Zu, Solid State Commun. 145 (2008) 15.
[84] L. Liang, X. Hui, C.M. Zhang, G.L. Chen, Intermetallics 16 (2008) 198.
[85] L. Liang, X. Hui, G.L. Chen, Mater. Sci. Eng. R 147 (2008) 13.
[86] M.E. Wood, W.H. Potter, Cryogenics 25 (1985) 667.
[87] X. Bohigas, J. Tejada, A. del Moral, Appl. Phys. Lett. 81 (2002) 2427.
[88] P.J. von Ranke, V.K. Pecharsky, K.A. Gschneidner, Phys. Rev. B 58 (1998) 12110.
[89] T. Hashimoto, T. Kuzuhara, M. Sahashi, K. Inomata, A. Tomokiyo, H. Yayama, J. Appl. Phys. 62 (1987) 3873.
[90] Z. Yan, J. Chen, J. Appl. Phys. 72 (1992) 1.
[91] G.S. Burkhanov, O.D. Chistyakov, Sov. Tech. Phys. Lett. 17 (1991) 353.
[92] Y. Zhang, Y.F. Ji, D.Q. Zhao, Y.X. Zhuang, R.J. Wang, M.X. Pan, Y.D. Dong, W.H. Wang, Scr. Mater. 44 (2001) 1107.
[93] Y. Zhang, D.Q. Zhao, R.J. Wang, W.H. Wang, Acta Mater. 51 (2003) 1971.
[94] [a] W.H. Wang, H.Y. Bai, R.J. Wang, D. Jin, Phys. Rev. B 62 (2000) 25;
[b] W.H. Wang, R.J. Wang, D.Q. Zhao, M.X. Pan, Appl. Phys. Lett. 74 (1999) 1803;
[c] W.H. Wang, M.P. Macht, H. Wollenberger, Appl. Phys. Lett. 71 (1997) 58;
[d] W.H. Wang, Q. Wei, M.P. Macht, H. Wollenberger, Appl. Phys. Lett. 71 (1997) 1053.
[95] L.M. Wang, W.H. Wang, R.J. Wang, Z.J. Zhan, D.Y. Dai, L.L. Sun, W.K. Wang, Appl. Phys. Lett. 77 (2000) 1147.
[96] L.M. Wang, L.L. Sun, W.H. Wang, W.K. Wang, Appl. Phys. Lett. 77 (2000) 3734.
[97] W.H. Wang, P. Wen, Y. Zhang, M.X. Pan, R.J. Wang, Appl. Phys. Lett. 79 (2001) 3947.
[98] W.H. Wang, R.J. Wang, W.T. Yang, B.C. Wei, P. Wen, D.Q. Zhao, M.X. Pan, J. Mater. Res. 17 (2002) 1385.
[99] P. Wen, R.J. Wang, W.H. Wang, J. Mater. Res. 17 (2002) 1785.
[100] R.J. Wang, F.Y. Li, W.H. Wang, Z.C. Qin, J. Phys. Condens. Mat. 14 (2002) 11311.
[101] L.M. Wang, R.J. Wang, W.H. Wang, W.K. Wang, J. Phys. C 15 (2003) 101.
[102] R.J. Wang, W.H. Wang, F.Y. Li, L.M. Wang, J. Phys. C 15 (2003) 603.
[103] Z. Bian, R.J. Wang, M.X. Pan, W.H. Wang, Adv. Mater. 15 (2003) 616.
[104] [a] Z. Zhang, R.J. Wang, M.X. Pan, W.H. Wang, J. Phys. C 15 (2003) 4503;
[b] Z. Bian, M.X. Pan, Y. Zhang, W.H. Wang, Appl. Phys. Lett. 81 (2002) 4739;
[c] Z. Zhang, L. Xia, Ru Ju Wang, B.C. Wei, M.X. Pan, W.H. Wang, Appl. Phys. Lett. 81 (2002) 4371;
[d] W.H. Wang, M.X. Pan, D.Q. Zhao, Y. Hu, H.Y. Bai, J. Phys. Condens. Mat. 16 (2004) 3719.
[105] W.H. Wang, J. Appl. Phys. 99 (2006) 093506.
[106] D. Schreiber, Elastic Constants and their Measurement, McGraw-Hill, New York, 1973.
[107] D.E. Gray, American Institute of Physics Handbook, third ed., McGraw-Hill, New York, 1973 (Chapter 3).
[108] H.S. Chen, J.T. Krause, E. Coleman, J. Non-Cryst. Solids 18 (1975) 157.
[109] W.H. Wang, J. Non-Cryst. Solids 351 (2005) 1481.
[110] W.L. Johnson, K. Samwer, Phys. Rev. Lett. 95 (2005) 195501.
[111] Y.H. Liu, G. Wang, D.Q. Zhao, M.X. Pan, W.H. Wang, Science 315 (2007) 1385.
[112] A.L. Greer, Science 267 (1995) 1947.
[113] T. Egami, Mater. Sci. Eng. A 226 (1997) 261.
[114] T. Egami, Rep. Prog. Phys. 47 (1984) 1601.
[115] W.H. Wang, D.Q. Zhao, M.X. Pan, P. Wen, J. Mater. Res. 18 (2003) 2747.
[116] J. Schroers, A. Masuhr, W.L. Johnson, R. Busch, Phys. Rev. B 60 (1999) 11855.
[117] W.H. Wang, W. Utsumi, X.L. Wang, Phys. Rev. B 70 (2004) 092203.
[118] R. Bruning, K. Samwer, Phys. Rev. B 46 (1992) 11318.
[119] V.N. Novikov, A.P. Sokolov, Nature 431 (2004) 961.
[120] V.N. Novikov, A.P. Sokolov, Phys. Rev. B 74 (2006) 064203.
[121] M. Jiang, L. Dai, Phys. Rev. B 76 (2007) 093506.
[122] M.L. Lind, G. Duan, W.L. Johnson, Phys. Rev. Lett. 97 (2006) 015501.
[123] P. Yu, R.J. Wang, D.Q. Zhao, H.Y. Bai, Appl. Phys. Lett. 90 (2007) 251904.
[124] P. Yu, R.J. Wang, D.Q. Zhao, H.Y. Bai, Appl. Phys. Lett. 91 (2007) 201911.
[125] R. Tarumi, M. Hirao, T. Ichitsubo, E. Matsubara, J. Saida, H. Kato, Phys. Rev. B 76 (2007) 104206.
[126] R.J. Wang, F.Y. Li, J.F. Wang, W.H. Wang, Appl. Phys. Lett. 83 (2003) 2814.
[127] E.F. Lambson, W.A. Lambson, J.E. Macdonald, M.R.J. Gibbs, G.A. Saunders, D. Turnbull, Phys. Rev. B 33 (1986) 2380.
[128] W.H. Wang, F.Y. Li, M.X. Pang, D.Q. Zhao, R.J. Wang, Acta Mater. 52 (2004) 715.
[129] B. Zhang, R.J. Wang, W.H. Wang, Phys. Rev. B 72 (2005) 104205.
[130] F.D. Murnaghan, Proc. Natl. Acad. Sci. USA 30 (1944) 244.
[131] S. Sen, S. Gaudio, B.G. Aitken, C.E. Lesher, Phys. Rev. Lett. 97 (2006) 025504.
[132] T. Morishita, Phys. Rev. Lett. 93 (2004) 055503.
[133] V.V. Brazhkin, A.G. Lyapin, J. Phys. Condens. Mat. 15 (2003) 6059.
[134] P.F. McMillan, J. Mater. Chem. 14 (2004) 1506.
[135] O. Mishima, L.D. Calvert, E. Whalley, Nature 314 (1985) 76.
[136] C. Meade, R.J. Hemley, H.K. Mao, Phys. Rev. Lett. 69 (1992) 1387.
[137] Y. Katayama, T. Mizutani, W. Utsumi, O. Shimomura, M. Yamakata, K. Funakoshi, Nature 403 (2000) 170.
[138] H.W. Sheng, H.Z. Liu, Y.Q. Cheng, J. Wen, P.L. Lee, W.K. Luo, S.D. Shastri, E. Ma, Nature Mater. 6 (2007) 192.
[139] P. Söerlind, Adv. Phys. 47 (1998) 959.
[140] Q.S. Zeng, Y.C. Li, C.M. Feng, P. Liermann, M. Somayazulu, G.Y. Shen, H.K. Mao, R. Yang, J. Liu, T.D. Hu, J.Z. Jiang, PNAS 104 (2007) 13565.
[141] X.R. Liu, S.M. Hong, Appl. Phys. Lett. 88 (2006) 042505.
[142] K. Binder, A.P. Young, Rev. Mod. Phys. 58 (1986) 801.
[143] D.X. Li, Y. Ōnuki, Phys. Rev. B. 57 (1998) 7434.
[144] H. Wang, T. Zhu, K. Zhao, W.N. Wang, C.S. Wang, Y.J. Wang, W.S. Zhan, Phys. Rev. B 70 (2004) 092409.
[145] E. Bonetti, L. Del Bianco, D. Fiorani, D. Rinaldi, R. Caciuffo, A. Hernando, Phys. Rev. Lett. 83 (1999) 2829.
[146] W. Bao, S. Raymond, S.M. Shapiro, K. Motoya, B. Fak, R.W. Erwin, Phys. Rev. Lett. 82 (1999) 4711.
[147] J. Dho, W.S. Kim, N.H. Hur, Phys. Rev. Lett. 89 (2002) 027202.
[148] D.X. Li, S. Nimori, Y. Shiokawa, Y. Haga, E. Yamamoto, Y. Onuki, Phys. Rev. B 68 (2003) 172405.
[149] R.A. Pelcovitis, E. Pytte, J. Rudnick, Phys. Rev. Lett. 40 (1978) 476.
[150] C. Jayaprakash, S. Kirkpatrick, Phys. Rev. B 21 (1980) 4072.
[151] R. Fisch, Phys. Rev. B. 42 (1990) 540.
[152] [a] E.M. Chudnovsky, W.M. Saslow, R.A. Serota, Phys. Rev. B 33 (1986) 251;
[b] E.M. Chudnovsky, J. Appl. Phys. 64 (1988) 5770.
[153] [a] B. Dieny, B. Barbara, Phys. Rev. Lett. 57 (1986) 1169;
[b] D.J. Sellmyer, S. Nafis, Phys. Rev. Lett. 57 (1986) 1173.
[154] R.I. Bewley, R. Cywinski, Phys. Rev. B 54 (1996) 15251.
[155] F. Bert, V. Dupuis, E. Vincent, J. Hammann, J.-P. Bouchaud, Phys. Rev. Lett. 92 (2004) 167203.
[156] D. Petit, L. Fruchter, I.A. Campbell, Phys. Rev. Lett. 88 (2002) 207206.
[157] T. Saito, Y. Matsumaru, K. Shinagawa, T. Tsushima, J. Magn. Magn. Mater. 130 (1994) 347.
[158] O.V. Billoni, S.A. Cannas, F.A. Tamarit, Phys. Rev. B 72 (2005) 104407.
[159] J.H. Chen, T.C. Lubensky, Phys. Rev. B 16 (1977) 2106.
[160] A. Chakrabarti, Phys. Rev. B 36 (1987) 5747.
[161] J.A. De Toro, M.A. López de la Torre, J.M. Riveiro, A. Beesley, J.P. Goff, M.F. Thomas, Phys. Rev. B 69 (2004) 224407.
[162] Q. Luo, D.Q. Zhao, M.X. Pan, W.H. Wang, Appl. Phys. Lett. 92 (2008) 011923.
[163] J.R.L. de Almeida, D.J. Thouless, J. Phys. A 11 (1978) 983.
[164] G. Kotliar, H. Sompolinsky, Phys. Rev. Lett. 53 (1984) 1751.
[165] A.T. Ogielski, Phys. Rev. B. 32 (1985) 7384.
[166] M.B. Tang, D.Q. Zhao, M.X. Pan, W.H. Wang, J. Non-Cryst. Solids 351 (2005) 2572.
[167] Y. Li, H.Y. Bai, P. Wen, Z.X. Liu, Z.F. Zhao, J. Phys. C 15 (2003) 4809.
[168] N. Mattern, U. Kühn, H. Hermann, S. Roth, H. Vinzelberg, J. Eckert, Mater. Sci. Eng. A 375–377 (2004) 351.
[169] O. Haruyama, N. Annoshita, N. Nishiyama, H.M. Kimura, A. Inoue, Mater. Sci. Eng. A 375–377 (2004) 288.
[170] J. Guo, F.Q. Zu, Z.H. Chen, Solid State Commun. 135 (2005) 103.
[171] J. Guo, F.Q. Zu, Z.H. Chen, X.F. Li, Y. Xi, R.R. Shen, Y. Zhang, J. Non-Cryst. Solids 352 (2006) 3859.
[172] Y.S. Ji, S.J. Chung, K.T. Hong, J. Yoon, G. Kim, Y.S. Ji, B.S. Seong, K.S. Lee, Mater. Sci. Eng. A 449–451 (2007) 521.
[173] S.J. Chung, K.T. Hong, M.O.J. Yoon, G. Kim, Y.S. Ji, B.S. Seong, K.S. Lee, Scr. Mater. 53 (2005) 223.
[174] H.Y. Bai, C.Z. Tong, P. Zheng, J. Appl. Phys. 95 (2004) 1296.
[175] G.R. Stewart, Rev. Mod. Phys. 78 (2006) 743.
[176] F. Steglich, J. Low Temp. Phys. 95 (1994) 3.
[177] A. Amato, Rev. Mod. Phys. 69 (1997) 1119.
[178] E. Miranda, V. Dobrosavljevic, G. Kotliar, Phys. Rev. Lett. 78 (1997) 290.
[179] A.H. Castro Neto, G. Castilla, B.A. Jones, Phys. Rev. Lett. 81 (1998) 3531.
[180] B. Andraka, G.R. Stewart, Phys. Rev. B 47 (1993) 3208.
[181] M.C. Aronson, R. Osborn, R.A. Robinson, J.W. Lynn, R. Chau, C.L. Seaman, M.B. Maple, Phys. Rev. Lett. 75 (1995) 725.
[182] O.O. Bernal, D.E. MacLaughlin, H.G. Lukefahr, B. Andraka, Phys. Rev. Lett. 75 (1995) 2023.
[183] M.B. Maple, J. Low Temp. Phys. 99 (1995) 223.
[184] J.S. Kim, J. Alwood, D. Mixson, P. Watts, G.R. Stewart, Phys. Rev. B 66 (2002) 134418.
[185] A.H. Castro Neto, B.A. Jones, Phys. Rev. B 62 (2000) 14975.